Hydrology Research

Hydrology Research Vol 56 No 11, 1137 doi: 10.2166/nh.2025.007

Assessment of drought vulnerability in the Nile River basin using satellite remote sensing, Africa

Agegnehu Kitanbo Yoshe [a,b,c]

[a]Department of Water Resources and Irrigation Engineering, Arba Minch University, 21 Post Office Box, Arba Minch, Ethiopia
[b]Siberian School of Geosciences Irkutsk National Research Technical University: Irkutsk, Siberia, Russia
[c]Journal of Asian Scientific Research: New York City, New York 10018, USA
E-mail: kitanbo@gmail.com; agegnehu.kitanbo@amu.edu.et

AKY, 0000-0002-3792-5854

ABSTRACT

The variation in water storage leads to frequent recurrence of droughts in the world, which causes societal, economic, and environmental impacts. In this research, the gravity recovery and climate experiments (GRACE) terrestrial water storage variation (TWS) was used to suggest drought events and compared with commonly used drought indices. The cross-wavelet coherence analysis was applied to further identify the possible multiscale relationships between TWS and chamite variables. From the perspective of drought events, 12 were observed based on estimated water storage deficit between 2002 and 2023 in the Nile River basin, and out of the 12 confirmed drought events, the periods between October 2003 and July 2007 and between September 2008 and September 2012 were the most extensive drought periods in the study region, with durations of 45 and 49 months, respectively. The multiscale relationship between the GRACE-based drought index (GDI) and the corresponding drought indices was detected using a cross-wavelet spectrum to understand its correlations. The evaluated GDI significantly correlated with meteorological drought. Finally, this study verified the importance of utilizing GRACE data for drought quantification and characterization.

Key words: Global Land Data Assimilation System (GLDAS), GRACE-based drought index, meteorological drought indices, R-studio, spatio-temporal variation of water storage, water deficit drought index

HIGHLIGHTS

- The long-term total water storage anomalies (TWSA) using GRACE (Gravity Recovery and Climate Experiment) and GRACE-FO (Follow-On) satellites were evaluated.
- The GRACE-based drought index (GDI) in the Nile River basin based on the GRACE satellite mission terrestrial water storage data product was developed, and it was compared with standardized drought indices (SPI and SPEI) to understand the combined effects of climate change and human activities.
- The multiscale relationship between the GDI and the corresponding drought indices was detected using cross-correlation.

GRAPHICAL ABSTRACT

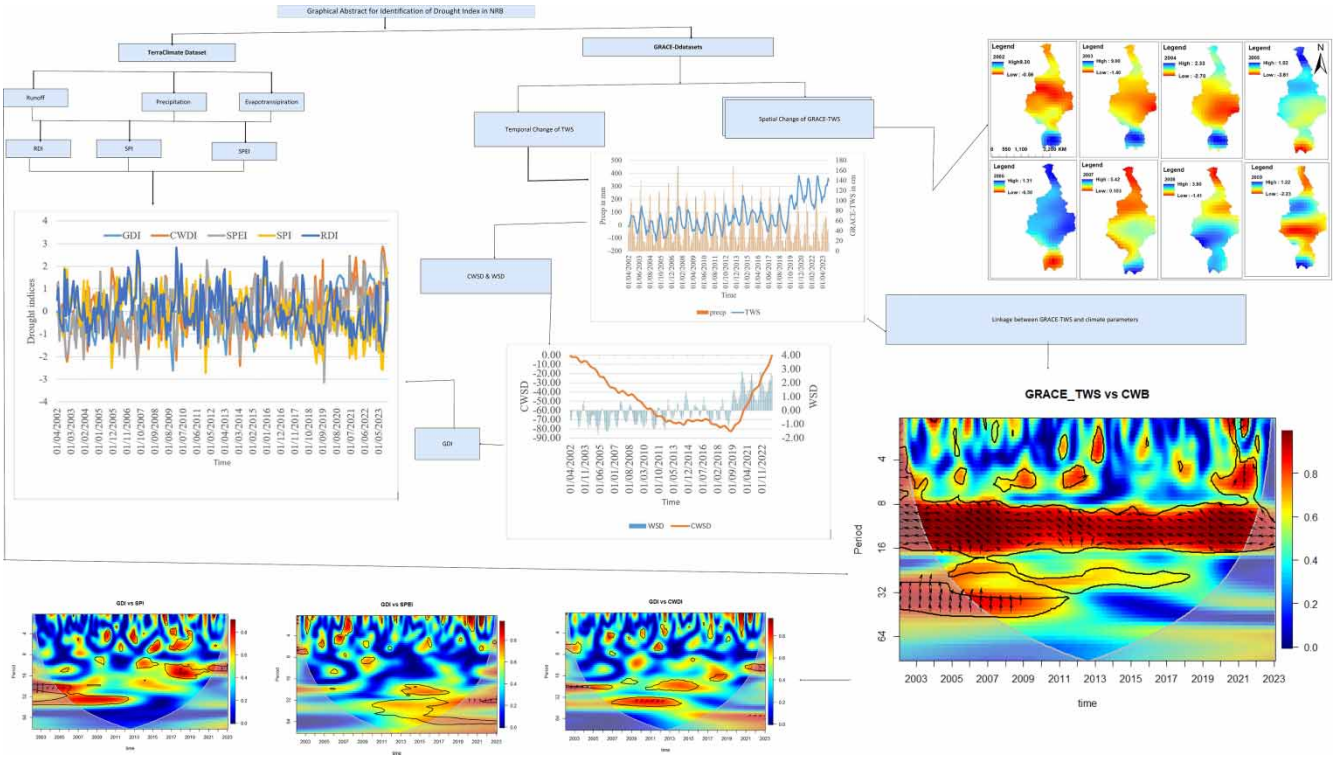

1. INTRODUCTION

Drought is one of the most common natural disasters in the world, which has the characteristics of high frequency and long duration and significantly affects agriculture, ecosystems, and socioeconomic development (Zargar *et al.* 2011; Mera 2018; Pendergrass *et al.* 2020; Wu *et al.* 2021). The frequent occurrence and long-term persistence of drought will not only bring enormous losses to industrial and agricultural production but also cause many adverse effects, such as water resource shortages, land desertification, and ecological environmental deterioration (Stanke *et al.* 2013; Dabanli 2018; Li *et al.* 2021). Droughts can also vary in multiple dynamic dimensions, including severity and duration, which makes them difficult to characterize (Valiya Veettil & Mishra 2020; Wu *et al.* 2022). Therefore, it is crucial and urgent to monitor and evaluate drought effectively.

Different researchers evaluated the spatial distribution of drought based on the station-observed meteorological and hydrological data (Yihdego *et al.* 2019). However, due to the spatial heterogeneity of the regional environment and the scarcity of station observation data, the accuracy of drought distribution characteristics obtained by spatial interpolation is not very high, which makes it difficult to reflect the large-scale dynamic drought information. In addition, some drought indices are only calculated by using a single variable (e.g., precipitation, soil moisture, or surface runoff), which may not reflect the actual situation of a drought disaster accurately and comprehensively (Thomas *et al.* 2014). Additionally, field measurements involve huge computational costs and significant financial resources and are also limited to either surface or groundwater zones data (Creutzfeldt *et al.* 2012).

Due to the rapid development of earth observation based on remote sensing technology (AghaKouchak 2015; Gao *et al.* 2015; Alizadeh & Nikoo 2018), the launch of the Recovery and Climate Experiment (GRACE) satellite mission cooperatively developed to speculate global water storage by making detailed measurements of the earth's gravity field (Tapley *et al.* 2004, 2019; Long *et al.* 2017; Xie *et al.* 2019; Yoshe 2023, 2024a, b). Compared with the conventional univariate indicator, GRACE-obtained terrestrial water storage (TWS) includes surface water storage, groundwater storage, soil moisture storage, snow water equivalent, and canopy water storage (Zhong *et al.* 2019). Thus, the development of GRACE gravity satellite technology has realized the dynamic observation of large-scale regional water resources changes, which can reflect all water resources

information (i.e., groundwater, surface water, soil moisture, etc.) and provide an additional data source for drought studies. Also, GRACE breaks the limitation of traditional ground observation on the temporal and spatial scale and has been widely used in regional drought investigation (Wang *et al.* 2019). Therefore, the GRACE satellites provide a new way for the retrieval of TWS changes (TWSC) (Tapley *et al.* 2004; Wahr *et al.* 2004) and also extend a new approach to the study of hydrological drought. Also, the GRACE-based drought severity index (GDI) provides a perspective on drought events based on TWS (Zhao *et al.* 2017). Sinha *et al.* (2019) combined TWSA from GRACE with rainfall analysis to construct the combined climatological deviation index to study drought in Indian river basins. It is also problematic to assess drought using rainfall or other surface water observations solely, since ongoing water loss from deeper storage can still occur even after surface water has become dry (Leblanc *et al.* 2009). Therefore, it is essential to evaluate the GRACE-based drought index (GDI) for the study area based on TWS variation.

To better monitor and quantify drought, the use of drought indices, calculated by assimilating drought indicators into a single numerical value, has become prevalent in drought characterization (Tsakiris *et al.* 2007). A drought index provides a comprehensive picture of drought analysis and decision-making that is more readily practical compared with raw data obtained from various drought indicators. Currently, different drought indices have been developed (Yi & Wen 2016). Zargar *et al.* (2011) reviewed 74 operational and proposed drought indices, emphasizing the popular drought indices. Among the various drought indices reported, the standardized precipitation index (SPI) (McKee *et al.* 1993), the standardized runoff index (SRI) (Shukla & Wood 2008), and the standardized precipitation evapotranspiration index (SPEI) (Abatzoglou *et al.* 2018) are the most widely used indices. Remote sensing-based drought indices have opened a new path forward in drought monitoring and detection (Niemeyer 2008), allowing accurate spatial information to be obtained with global or regional coverage with high reliability and a high repetition rate. In recent years, research on drought indices has started to integrate GRACE data to measure the occurrence, severity, frequency, magnitude, and duration of hydrological droughts based on the GRACE-derived TWS (Thomas *et al.* 2014; Wang *et al.* 2014).

Several researchers have evaluated drought indices in the Nile River basin (Bayissa *et al.* 2021; Nigatu *et al.* 2024). Nigatu *et al.* (2024) evaluated meteorological, agricultural, and groundwater propagation. However, there are no studies applying GRACE-based TWS deficit to characterize drought index in the Nile River basin. The general objective of this study is to develop a GDI in the Nile River basin based on the GRACE satellite mission TWS data product and compare it with standardized drought indices (SPI and SPEI) to understand the combined effects of climate change and human activities. The specific objectives of this study were to evaluate changes in TWS anomalies (TWSA) from GRACE satellite datasets.

- ❖ To evaluate the WSD based on GRACE-TWSA obtained, and its importance as a tool to evaluate drought events in the Nile River basin.
- ❖ To evaluate the GDI based on the estimated WSD.
- ❖ To estimate drought severity based on estimated GDI and its comparison with other drought indices such as SPI, the reconnaissance drought index (RDI), climatic water balance drought index (CWBDI), and SPEI.

Overall, this study provides reliable outcomes that will be vital for establishing climate change adaptation pathways in the future for viable water resources management to minimize the disastrous impacts of drought in the Nile River basin. Therefore, the adopted approaches and methodology for evaluating drought indices and obtaining results will be regarded as a new and valuable contribution to the present study area. The research was based on available GRACE datasets between 2002 and 2023.

2. MATERIAL AND METHODS

2.1. Description of the study area

The Nile River is located in eastern Africa and flows into the Mediterranean Sea (Figure 1). Its drainage basin includes 11 countries in East Africa: the Democratic Republic of the Congo, Tanzania, Burundi, Rwanda, Uganda, Kenya, Ethiopia, Eritrea, South Sudan, the Republic of the Sudan, and Egypt, with a total drainage area of 3,349,00 km^2 and a total length of 6,650 km. The Nile has two major tributaries: the White Nile, which begins at Lake Victoria and flows through Uganda and South Sudan; and the Blue Nile, which begins at Lake Tana in Ethiopia and flows into Sudan from the southeast. The two rivers meet in the Sudanese capital of Khartoum (Camberlin 2009; Hamouda *et al.* 2009). Figure 1 shows the location map of the study area. There has been a drought in the past few decades as a result of climate change, population growth, and urbanization, which has impacted the work being done on development in the Nile River basin. Annual precipitation in excess of

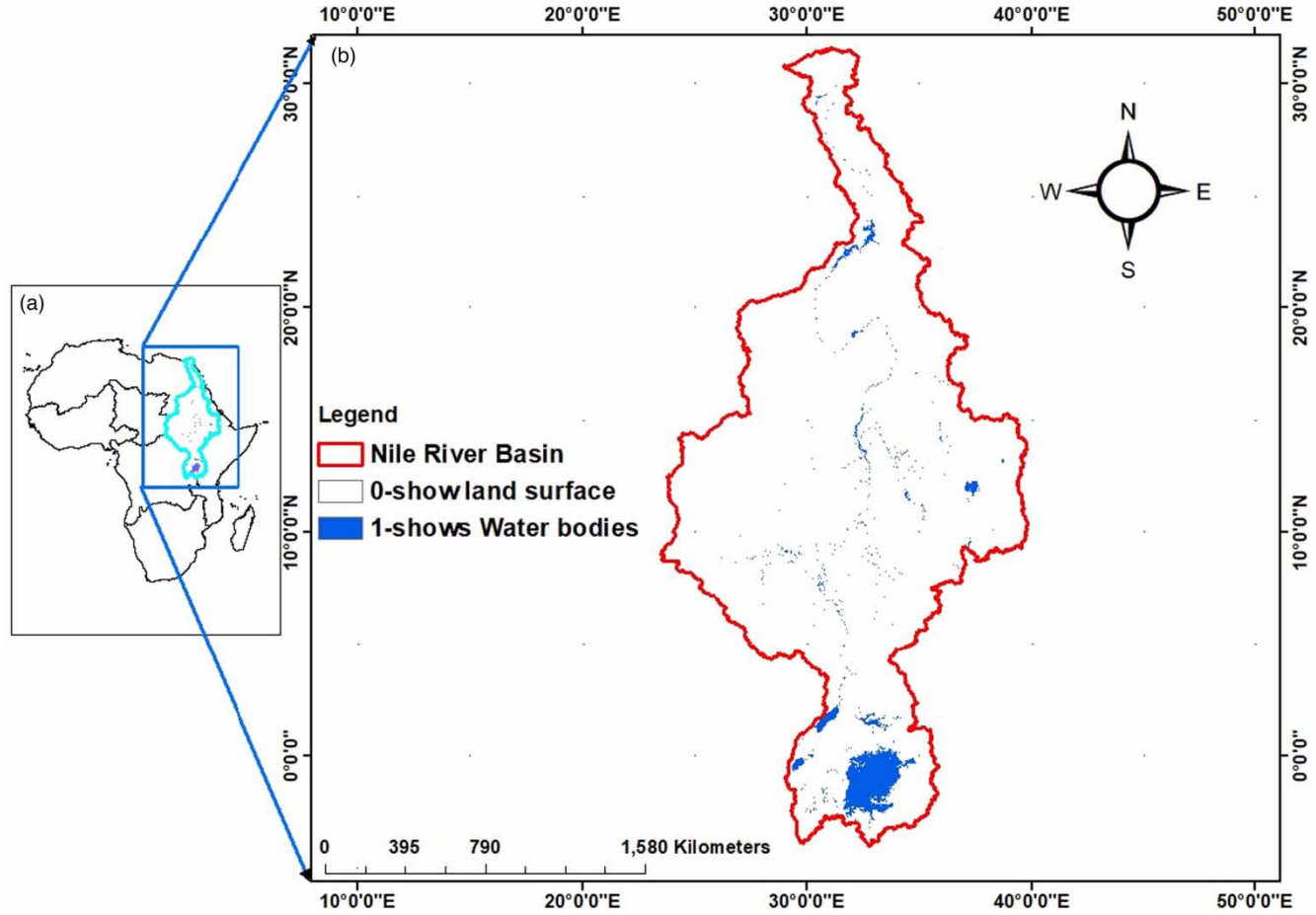

Figure 1 | Location map of the study area. (a) Level 02 hydro basins of Africa and (b) study area.

1,000 mm is restricted mainly to the equatorial region and the Ethiopian highlands (Camberlin 2009). From northern Sudan to all across Egypt, precipitation is negligible, below 50 mm/year, except along the Mediterranean coast.

2.2. Data collection

To evaluate drought indices in the Nile River basin, different datasets were utilized, like the GRACE satellite-based dataset and the TerraClimate dataset. The GRACE datasets were collected from three different institutions, namely, CSR (University of Texas/Center for Space Research), GFZ (GeoForschungsZentrum Potsdam), and JPL (NASA Jet Propulsion Laboratory). The GRACE dataset was presented at one-degree spatial resolution from 1 April 2002 to 7 January 2017 (Swenson & Wahr 2002, 2006; Landerer & Swenson 2012; Swenson 2012). To obtain an accurate original signal that was lost during data processing, a multiplicative scaling factor was used for the monthly data provided by the GRACE product (Seyoum *et al.* 2019; Yoshe 2023, 2024a, b, 2025). TerraClimate is a dataset of monthly climate and climate water balances for the global terrestrial surface. The TerraClimate datasets were available from 1958 to 2022 (Abatzoglou *et al.* 2018). The available data used for evaluation of drought index in the Nile River basin was presented in Table 1.

2.3. Methodology

The evaluation of drought index using remote sensing data is currently used by most scholars (Yirdaw *et al.* 2008; Thomas *et al.* 2014; Chao & Ding 2016; Forootan *et al.* 2016; Yi & Wen 2016; Zhang *et al.* 2016; Zhao *et al.* 2017; Sun *et al.* 2018; Seka *et al.* 2022). First, available datasets were collected, and WSD was evaluated from GRACE-based TWS; then, cross-wavelet coherence analysis was applied to identify the possible linkage between TWS and climate variables. For this study, the GDI was evaluated using GRACE-TWS and standardized using R-Studio. Additionally, the commonly used drought

Table 1 | Available data used for evaluation of drought index in the Nile River basin

Parameters	Source and processing	Unit	Converted to
TerraClimate precipitation	Precipitation (Precp) at (0.5° × 0.5°)	mm	
TerraClimate temperature	Temperature (Tm) (0.5° × 0.5°)	°C	
GRACE-TWS	GRACE satellite (CSR, JPL, GFZ) at (1° × 1°)	cm	Mm
TerraClimate evapotranspiration	Evapotranspiration (0.5° × 0.5°)	mm	
TerraClimate soil moisture	Soil moisture (Sm) (0.5° × 0.5°)	mm	
TerraClimate runoff	Runoff (Ru) (0.5° × 0.5°)	mm	

indices, such as SPI, RDI, CWBDI, and SPEI, were evaluated. Finally, WaveletComp was applied to identify the correlation between the GDI and the commonly used drought indices. Figure 2 shows the generalized methodology applied in this study for drought evaluation in the Nile River basin.

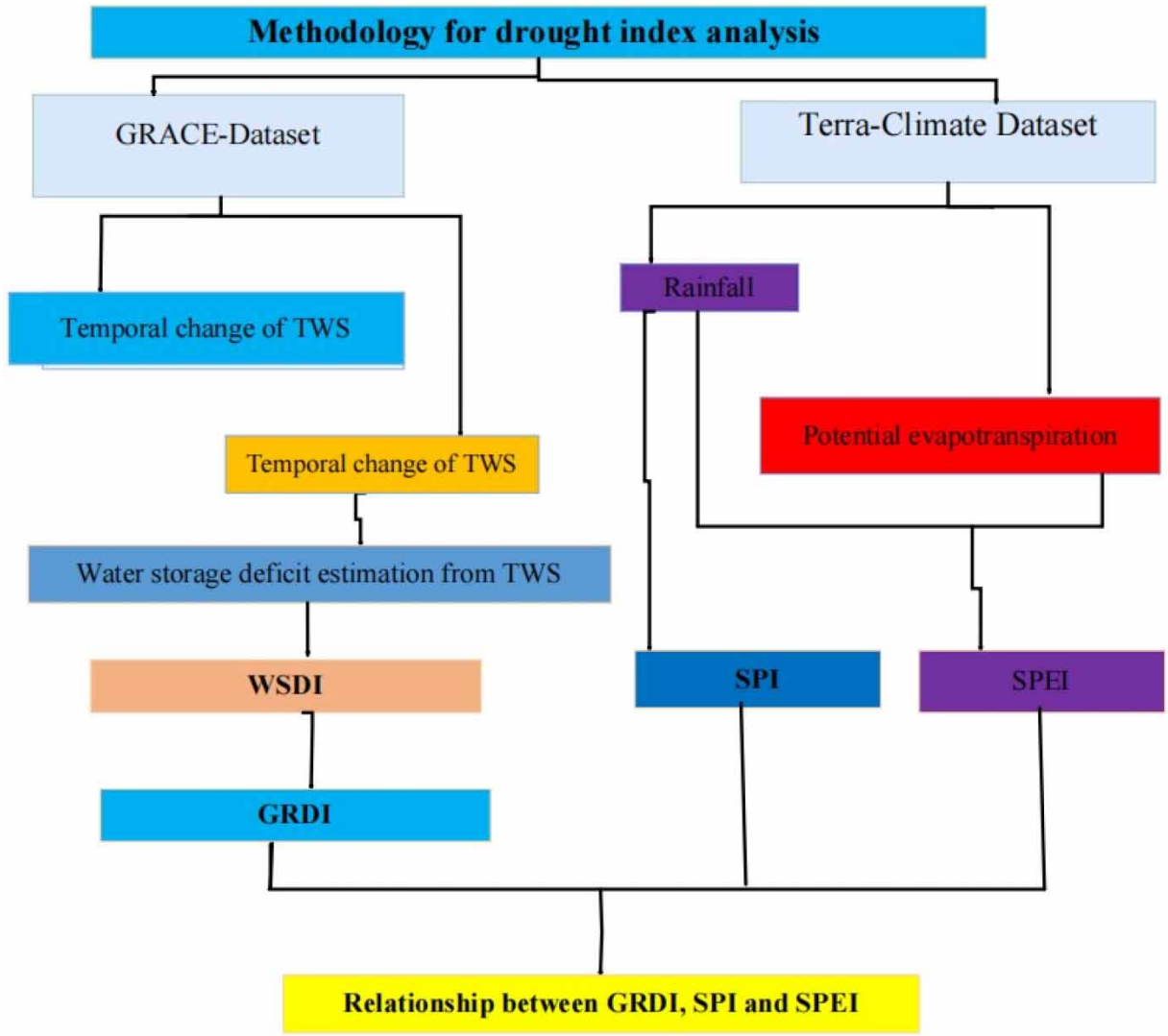

Figure 2 | Flow diagram of the methodology.

2.3.1. GRACE-derived drought indices

The proposed methodology for evaluating drought indices for this study is based on the data availability of GRACE from 2002 to 2016 (Swenson & Wahr 2006; Landerer & Swenson 2012). We produce spatial and temporal averaged GRACE-TWS time series. Estimation of TWS from the GRACE dataset has been widely adopted in the past few years (Dostdar *et al.* 2021; Yoshe 2023, 2024a, b). GRACE data processing and analysis for terrestrial water estimation were presented in previous studies (Yoshe 2023, 2024a, b). After TWS was estimated, the deficit in water storage was obtained as the difference between monthly TWS and the long-term mean of terrestrial water over the same month (Thomas *et al.* 2014; Thomas & Prasannakumar 2016; Sun *et al.* 2018; Yu *et al.* 2019), which is expressed in Equation (1).

$$\mathrm{WSD}_{k,p} = \mathrm{TWSA}_{k,p} - \mathrm{TWSA}_{k,p} \tag{1}$$

where $\mathrm{WSD}_{k,p}$ and $\mathrm{TWSA}_{k,p}$ are the deficit in water storage and GRACE-based TWSA time series in mm for month in the year k, respectively, is the long-period average of a month (the month in a year). A negative WSD shows loss of TWS as related to its monthly mean values, whereas a positive value indicates excessive amounts of water storage. If a negative WSD lasts for three or more consecutive months, it is intended to be a drought event (Thomas & Prasannakumar 2016). The GDI is computed by normalizing WSD, as presented in Equation (2).

$$\mathrm{GDI}_{k,p} = \frac{\mathrm{WSD}_{k,p} - \mu}{\sigma} \tag{2}$$

where $\mathrm{GDI}_{k,p}$ represents the GDI time series for the Pth month in the year k; μ is the average of the WSD time series; and δ is the standard deviation of the WSD. The WSD was standardized to provide the GDI for better characterization and comparison of GRACE-derived WSD with other standardized drought indices. Based on Thomas *et al.* (2014), the average WSD during the drought months of successive drought months was used to evaluate the drought brutality based on WSD, which can be described in Equation (3).

$$Sev = Mm(t) * Dd(t) \tag{3}$$

where $Sev(t)$ and $Mm(t)$ indicate the severity and the average WSD of drought events at duration t, respectively. $Dd(t)$ shows the number of consecutive months between the start and end of the drought events.

2.3.2. Standardized precipitation index

The proposed methodology for evaluating drought indices for this study is based on the data availability of TerraClimate from 1991 to the present (Abatzoglou *et al.* 2018). The SPI was used to characterize drought (McKee *et al.* 1993). This index evaluates drought conditions based only on precipitation and has proven to be effective for analyzing wet and dry periods (Espinosa *et al.* 2019). The SPI method stands out for its speed, great approximation in drought analysis, simplicity, and minimal data requirement (Ji & Peters 2003; Keyantash & Dracup 2004). A drought event is defined as the sum of consecutive months in which the SPI falls below a certain threshold for at least two consecutive months. In this study, a drought event starts when the SPI is equal to or below −1.0 and ends with the first positive SPI. Different time scales of 1-3-12 months (SPI-12) were analyzed to detect drought episodes at relatively short timescales and long-term (18–48) patterns for the study of episodes related to meteorological and hydrological droughts, groundwater stage, and the water resources in the region (WMO 2012). The gamma distribution analysis was applied to evaluate the cumulative probability of precipitation based on Hayes *et al.* (1999) and Cacciamani *et al.* (2007) equations. Then the cumulative probability obtained based on no precipitation events and the number of total data points (n) was transformed to the standard normal random variable value with zero average values and a variance equal to one based on the Vicente-Serrano *et al.* (2010) equation (Cacciamani *et al.* 2007).

2.3.3. Standardized precipitation evapotranspiration index

For potential evapotranspiration (PET) estimation based on PM (PET_{PM}), the Mesonet provides estimated daily PET data based on the ASCE Standardized reference equation as follows:

$$ET = \frac{\Delta(R_n - G) + \rho_a c_p \frac{(e_s - e_a)}{\gamma_a}}{\Delta + \gamma\left(1 + \frac{\gamma_s}{\gamma_a}\right)} \tag{4}$$

where Δ is the slope of the saturation vapor pressure curve, R_n is the net radiation, G is the soil heat flux, ρ_a is the air density, c_p is the specific heat of air, $e_s - e_a$ is the vapor pressure deficit, γ is psychrometric constant, and γ_s and γ_a are surface and aerodynamic resistance.

Then, to evaluate the SPEI value, the monthly deficit (Md) was estimated as follows:

$$D_i = P_i - PET_i \tag{5}$$

Once the D_i values are calculated, the values are aggregated at different time scales. The probability distribution (e.g., three-parameter log-logistic distribution) is fitted to the accumulated D_i series at each Mesonet station. The difference between precipitation and evapotranspiration is referred to as the climatic water balance (CWB) with the atmospheric evaporative demand (Beguería *et al.* 2014). Hereafter, SPEI-n represents SPEI with an n-month accumulation period. The SPEI values can be calculated by standardizing the cumulative D series as follows:

$$SPEI_i = W_i - \frac{2.515517 + 0.802853W_i + 0.010328W_i^2}{1 + 1.432788W_i + 0.189269W_i^2 + 0.001308W_i^3} \tag{6}$$

$$W_i = \sqrt{-2\ln p} \text{ for } P \leq 0.5 \tag{7}$$

$$W_i = \sqrt{-2\ln(1-p)} \text{ for } P > 0.5 \tag{8}$$

where p is the probability of exceeding a given D_i, and the sign of the resultant SPEI is reversed for $p > 0.5$. A detailed description of calculating the SPEI is provided by Vicente-Serrano *et al.* (2010).

The SPI and SPEI normalize the variation of precipitation in multiple accumulation periods from 1 to 48 months at a particular location using the long-term average. The shorter timescale of 1–6 months is used to monitor the occurrence of meteorological droughts, and the longer timescale of SPI from the 12 to 24 months accumulation period is often used as a proxy for agricultural as well as hydrological droughts (Munagapati *et al.* 2018; Cammalleri *et al.* 2019). Additionally, the other characteristics of drought, such as duration, intensity, and magnitude, were also computed using SPI methods. The drought magnitude for an area was evaluated by Equation (9).

$$DM = \sum_{i=1}^{n} SPI_{ij} \tag{9}$$

To avoid the negative value of DM, Equation (9) can be rewritten as in Equation (10)

$$DM = \left(\sum_{i=1}^{n} SPI_{ij}\right) * (-1) \tag{10}$$

where DM denotes the drought magnitude, and n represents the number of consecutive months per drought event on a j timescale. The ratio of drought magnitude over drought duration can be defined as drought intensity (DI) and expressed in

Equation (11).

$$\mathrm{DI} = \frac{\mathrm{DM}}{Dd(t)} \tag{11}$$

where $Dd(t)$ represents the duration of drought.

The severity of the drought is associated with evaporative water demand because of evapotranspiration as the temperature rises, which could be better identified using the SPEI (Homdee *et al.* 2016).

2.3.4. Surface runoff drought indices

The surface runoff drought index is a multivariate hydrological drought index that shows the potential of rainfall runoff for evaluating drought in the river basin. It is calculated by fitting a lognormal distribution function to the rainfall runoff (Shukla & Wood 2008). It is similar to SPI and dimensionless. For this study, we used the TerraClimate dataset to evaluate the characteristics of drought due to rainfall runoff. The entire SPI, SPEI, SRI, and GDI calculation process (including fitting parameters for probability density functions) was made with the 'SCI' package in the R programming language (Gudmundsson & Stagge 2016).

2.4. Wavelet coherence analysis for the estimated drought index

The wavelet coherence can be used to evaluate the coherence of the cross-wavelet transform in the time-frequency space (i.e., to estimate frequency bands and time intervals). In this study, a Torrence and Webster definition was applied, which shows the wavelet coherence of two time series as a function of the power spectrum density and the cross-spectrum density (Farge 1992; Grinsted *et al.* 2004). Equation (12) shows the wavelet coherence utilized to measure the correlation between the two series, primarily focusing on regions of low energy.

$$R_n^2(S) = \frac{|S*(S^{-1}W_n^{XY}(S))|^2}{S*(S^{-1}|W_n^X(S)|^2)*S(S^{-1}|W_n^Y(S)|^2)} \tag{12}$$

where S is the smoothing operator, $W_n^X(S)$ and $W_n^Y(S)$ are the wavelet transforms of the two time series X and Y, respectively, and $|W_n^{XY}(S)|$ is the cross-wavelet spectrum of X and Y.

Equation (13) shows that the cross-wavelet transform technique allows for the examination of shared power and coherence across two time series, identifying correlations within both frequency and time domains, especially in regions of high energy.

$$S(W)W_n^{XY} = W_n^X(S)W_n^{Y*}(S) \tag{13}$$

where W_n^{Y*} represents the complex conjugate, and W_n^Y illustrates the cross-wavelet power spectrum. The statistical significance level of the wavelet coherence is estimated using the WaveletComp package in R-Studio.

2.5. Drought severity characterization

These drought severity classes are used to describe the magnitude of drought events throughout the Nile River basin, as indicated in Table 2. Evaporative demand drought index (EDDI) is a drought index that only relies on potential evapotranspiration (Hobbins *et al.* 2016).

2.6. Evaluation of methods of model performance and its correlation analysis

To estimate the consistency and similarity of the three GRACE-based TWS (CSR, JPL, and GFZ data products) and the selected drought indices, Pearson's correlation coefficient was used here, as shown in Equation (20) (Rummel 1976). And to calculate the downscaled TWS results, four different statistical metrics were used, including mean absolute error (MAE), Nash-Sutcliffe efficiency (NSE), R, and root mean error (RME). The mathematical representation of MAE, NSE, R, and RME is shown in Equations (14)–(17) (Liu *et al.* 2012; Richey *et al.* 2015). For root-mean-square error (RMSE) and MAE, the values close to 0 indicate the perfect model, whereas in NSE and R, the values closer to 1 indicate the perfect

Table 2 | Characteristics of drought intensity for SPI, SPEI and GDI, EDDI

Drought condition	EDDI	SPI, SPEI, GDI, SRI
Extreme drought	≥2.0	≤− 2
Severe drought	1.5–1.99	−1.5 to −1.99
Moderate drought	1.0–1.49	−1.0 to −1.49
Near normal		
Mild drought	0.5–0.99	−0.99 to −0.5
Normal	$-0.5 \leq 0 \leq -0.5$	$-0.5 \leq 0 \leq 0.5$
Wild	−0.99 to −0.5	0.5–0.99
Moderate wet	−1.0 to −1.49	1.0–1.49
Very wet	−1.5 to −1.99	1.5–1.99
Extremely wet	≤− 2	≥2.0

Source: McKee *et al.* (1993), Hobbins *et al.* (2016), and Yu *et al.* (2019).

model (Liu *et al.* 2012).

$$\mathrm{RMSE} = \sqrt{\frac{\sum_{i=1}^{N}(X_i - Y_i)^2}{N}} \tag{14}$$

$$\mathrm{NSE} = 1 - \frac{\sum_{i=1}^{N}(Y_i - \bar{Y})^2}{\sum_{i=1}^{N}(X_i - \bar{X})^2} \tag{15}$$

$$R = \frac{\sum_{i=1}^{N}(X_i - \bar{X})(Y_i - \bar{Y})}{\sqrt{\sum_{i=1}^{N}(X_i - \bar{X})^2}\sqrt{\sum_{i=1}^{N}(Y_i - \bar{Y})^2}} \tag{16}$$

$$\mathrm{MAE} = \frac{1}{N}\left(\sum_{i=1}^{N}|Y_i - X_i|\right) \tag{17}$$

where X_i and Y_i indicate two independent datasets with the mean values of X and Y. The input TWS is represented by X_i, and the predicted value of a random forest model is represented by Y_i. While N represents the total number of samples.

$$r(\mathrm{GR}, \mathrm{GL}) = \frac{\sum_{i=1}^{N}(\mathrm{GR}_i - \overline{\mathrm{GR}})(\mathrm{GL}_i - \overline{\mathrm{GL}})}{\sqrt{\sum_{i=1}^{N}(\mathrm{GR}_i - \overline{\mathrm{GR}})^2}\sqrt{\sum_{i=1}^{N}(\mathrm{GL}_i - \overline{\mathrm{GL}})^2}} \tag{18}$$

where GR is the monthly TWS estimated from GRACE, GL is the monthly hydroclimatic factor calculated from GRACE, and N is the number of months.

3. RESULTS

3.1. Temporal variation of TWS and WSD

Generally, the change in rainfall affects the TWS animals. However, considering TWSA as an anomaly value, it is compared with precipitation and the observed monthly precipitation. Figure 3 demonstrates the time variations of TWSA and

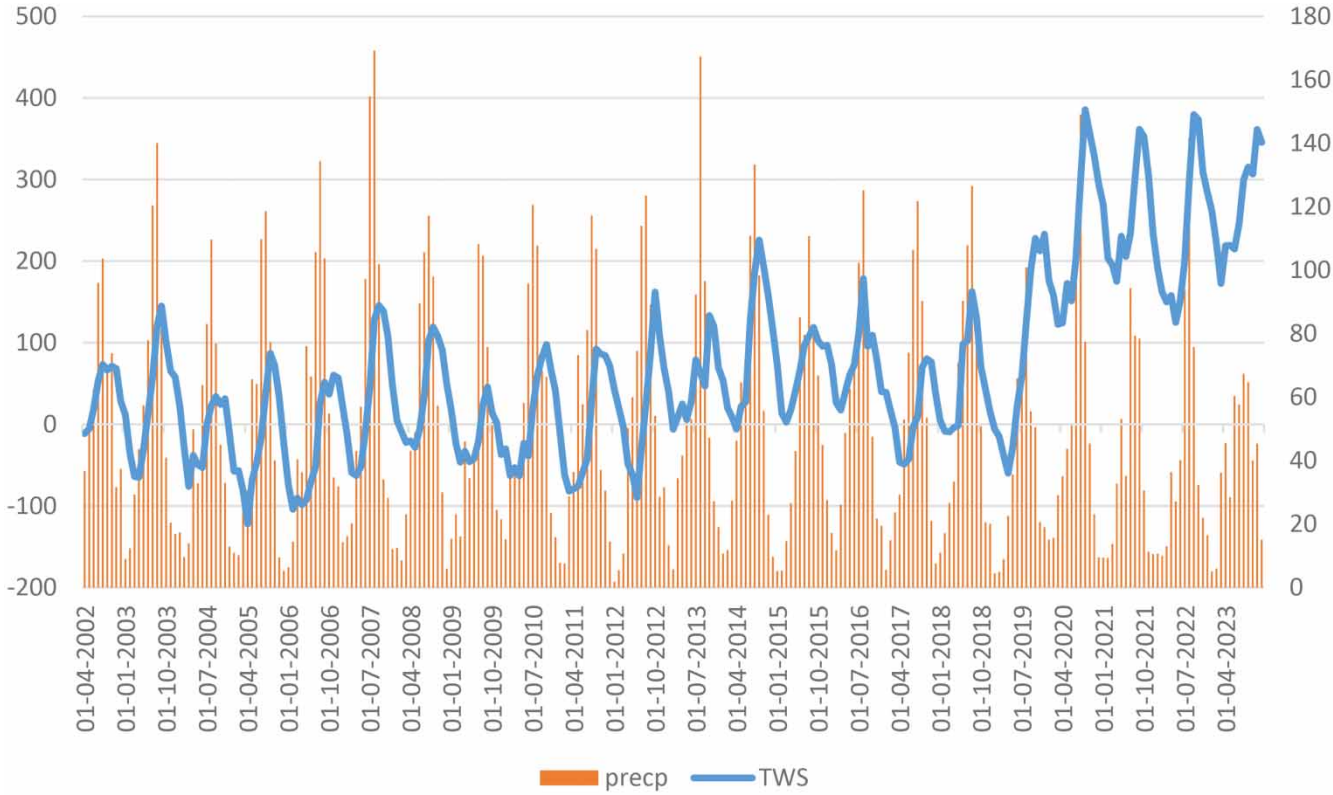

Figure 3 | Time series of GRACE-inferred total water storage anomaly (TWSA) and observed precipitation anomaly for the Nile River basin from 2002 to 2023.

precipitation annually from 2002 to 2023. It indicates that the majority of precipitation occurs in the summers of 2002 to 2023. The annual fluctuation of precipitation anomalies is in agreement with peaks in the TWSA time series in the study area during the study period. TWSA has a simultaneous change in trends from 2002 to 2017 and an increasing trend from 2017 to 2023. The trend of TWSA demonstrates that the Nile River basin became water surplus from 2017 to 2023. The change is similar to the combined effects of climatic factors. The precipitation trend has a decreasing trend from 2013 to 2023 and an increasing trend from 2002 to 2008, but no apparent trend in air temperature. The average TWSA was 69.23 cm, whereas the average precipitation from 2002 to 2023 was 50.51 mm. Thus, the change in TWSA might be attributed to climate change, with its effects on temperature, precipitation patterns, and evapotranspiration (Zhang *et al.* 2022; Palazzoli *et al.* 2025). The average TWSA indicates water resource gain during the study period.

The terrestrial WSD was estimated by GRACE-based TWS for the characterization of drought manifestation using Equation (1). The WSD shows a significant variation from 2002 to 2023 (Figure 4). The change of WSD can be classified into three stages: the first stage occurring from 2002 to 2012, the second stage from 2013 to 2019, and the third stage from 2020 to 2023. Extremely high water storage deficits occurred in the first stage, while water storage surpluses predominated in the third stage. The cumulative water storage deficit (CWSD) from 2002 to 2019 represents a continuous deficit and shows a continuous surplus from 2020 to 2023. A declining trend denotes a lasting WSD, and an upward trend represents a water storage surplus. Therefore, based on the result, the Nile River basin experienced long-term drought between 2002 and 2019, which is consistent with the previous study (Abd-Elbaky & Jin 2019). It is clear that TWS variation from GRACE was due to variability of precipitation, groundwater storage, soil moisture, canopy water storage, and surface water, which was also reported by similar studies (Tapley *et al.* 2004; Wang *et al.* 2020; Elsaka 2021; Elsaka *et al.* 2022). The correlation between cumulative precipitation and CWSD was 0.96, which shows that precipitation plays an important role in the variation of GRACE-TWS for the Nile River basin. The most extensive WSD that occurred in the study area coincided with the precipitation decline in the basin, climate variability, and human activities (urbanization, irrigation agriculture, dam construction, etc.) and other studies also confirmed that natural factors and human activities result in water storage variability

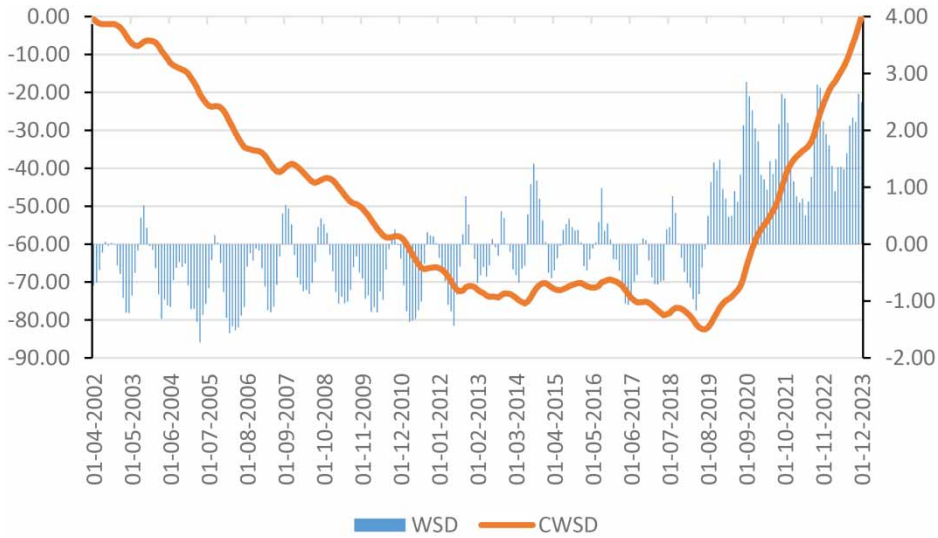

Figure 4 | Water storage deficit (WSD) and cumulative water storage deficit (CWSD).

(Philipps & McIntyre 2000; Segele & Lamb 2005; Onyutha & Willems 2015a). Therefore, a larger WSD shows a greater intensity of drought events, whereas a smaller WSD shows less intensity of drought events. This variability can most likely be due to the combined effect of climate change and human activities.

It is important to verify the accuracy of the results after evaluating TWS from GRACE. Thus, the GLDAS hydrological model is used for the verification of GRACE-based TWS. For this study, GLDAS TWS from 2010 to 2020 was used for the verification processes (Figure 5). Based on the evaluated results, the water storage changes (WSC) obtained from GRACE and GLDAS were basically consistent and had a significant correlation value of 0.85. The temporal variation of TWS is typically represented by its seasonal and interannual fluctuations, where rises during wet seasons and declines during dry periods can be clearly observed during the study period.

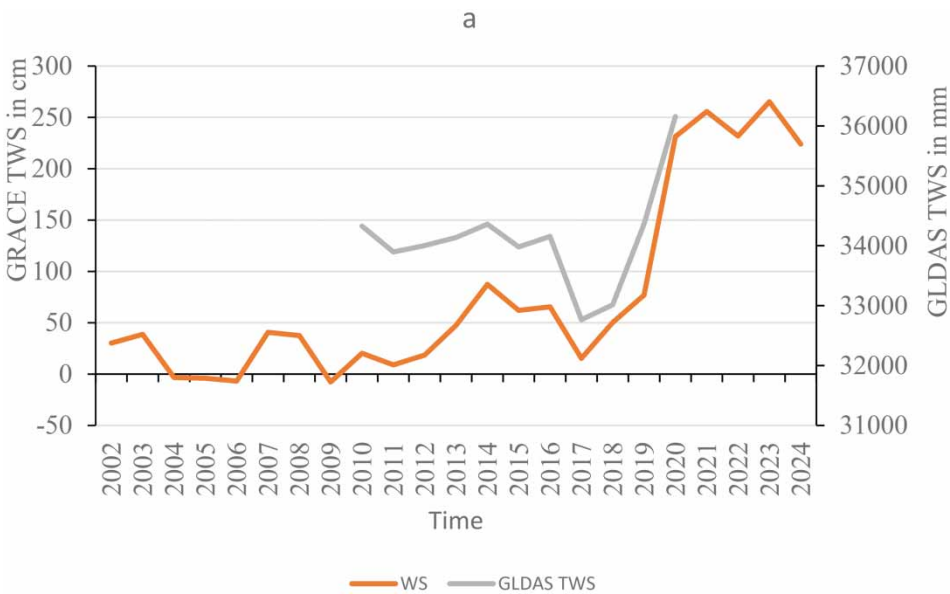

Figure 5 | Water storage change in the Nile River basin from 2002 to 2016: (a) annual variation of GRACE and GLDAS TWS.

3.2. Spatiotemporal change of TWS from GRACE

In this research, the spatial distribution of GRACE-based TWSA was examined for the study area from 2002 to 2016. Figure 6 shows variations in spatiotemporal maps of TWS variation for the Nile River basin, and observed that there was spatial variation during the study period. Terrestrial water is one of the most critical elements for all living creatures to survive and is essential for their life needs. Historical changes in water storage are vital for water management and water resource planning. The concept of drought is one of the biggest issues related to water availability under climate change. As presented in Figure 4, a significant change in TWS was observed for the Nile River basin at spatiotemporal levels during the study period. As presented in Figure 6, the maximum decrease in TWS between 2014 and 2015 was observed with a change of −24.7 cm/year, whereas the maximum increase was observed between 2006 and 2007 with a change of 14.96 cm/year. The spatiotemporal variation of TWS in the river basin was due to varying precipitation in the river basin, which agrees with similar studies (Yoshe 2023, 2024a, b). Other studies also agree with this finding, showing low precipitation in the northern parts of the river basin and high precipitation in the equatorial region and Ethiopia (Camberlin 2009).

3.3. Periodicity of GRACE-TWS and climate variables

The WaveletComp was performed to further identify the periodic oscillation of TWS from GRACE and climate parameters in the study area. The time series analysis between the GRACE-TWS and climate parameters like CWB, precipitation (precp), temperature (Tm), runoff (Ru), and soil moisture (Sm) was evaluated. These tests are performed using machine learning simulations. Supplementary material S1 shows a color-mapped wavelet power spectrum between the GRACE-TWS and selected climate parameters. It is shown in Supplementary material S1 that a red and yellow color shows a high degree of wavelet coherence between parameters, whereas the blue color indicates a low degree of coherence between the selected variables. The thick contours designate the 95% confidence level against red noise, whereas a black line shows the cone of influence. For the study area, a significant continuous wavelet power spectrum was observed for the first period bands from 2002 to 2023, showing varying trends based on frequency variations. The wavelet power spectrum for TWS, CWB, PET, soil moisture, temperature, precipitation, and runoff ranged from 0 to 8, 0 to 20.4, 0 to 19.1, 0 to 25.8, 0 to 18, 0 to 25, and 0 to 27.2, respectively. Based on the result, the analysis identifies that TWS from GRACE was affected by the variability of these climatic variables, like climate water balance, potential evapotranspiration, soil moisture, temperature, precipitation, and runoff, based on the periodicity of the climate variables (Supplementary material S1). The model performance was evaluated using Equations (14)–(17), and based on the results obtained, the value of R is 0.89, NSE is 0.85, MAE is 14.68 cm, and RMSE is 37.6 cm for the GRACE-TWS. The aim of analyzing model performance was to understand the characteristics of simulated and observed values with less error, and the obtained results showed good performance of the model.

3.4. Multiscale linkages between GRACE-TWS and climate variables

The cross-wavelet coherence analysis was applied to further identify the possible multiscale relationships and the local phase locking between GRACE-TWS and the corresponding climate variables in the Nile River basin. An arrow in the wavelet coherence plot represents the lead/lag phase relations between the examined series. A zero-phase difference means that the two time series move together on a particular scale. Arrows point to the right (left) when the time series are in-phase (anti-phase) (Figure 7). When the two series are in-phase, it indicates that they move in the same direction, and anti-phase means that they move in the opposite direction. Arrows pointing to the right or left indicate that the first variable is leading, while arrows pointing to the right up or left down show that the second variable is leading. Figure 6 shows the cross-wavelet coherence for the selected parameters during the study period. Based on the estimated result, for the frequency level of 1 month, the wavelet coherence has a very high scale for all variables. The arrow moves left up in the direction between TWS and CWB, left down between (TWS and PET, TWS and Tm), right down between (TWS and soil moisture, TWS and Precp, TWS and Runoff), right up between CWB and PET, and lifts between CWB and soil moisture. In general, a significant variation was observed between TWS and climate parameters in the study area during the study period at different frequency levels and confirming that the variability of climate change affects the TWS in the study area. Several studies have also explored the multiscale linkages between GRACE-TWS and various climate variables (Scanlon *et al.* 2021; Wei *et al.* 2021) and assessed the impact of climate change on water storage for enhancing freshwater reporting. Another study analyzed the spatial and temporal correlations between GRACE-TWS and climate indices to understand the relationships between large-scale climate patterns and regional WSC and employed

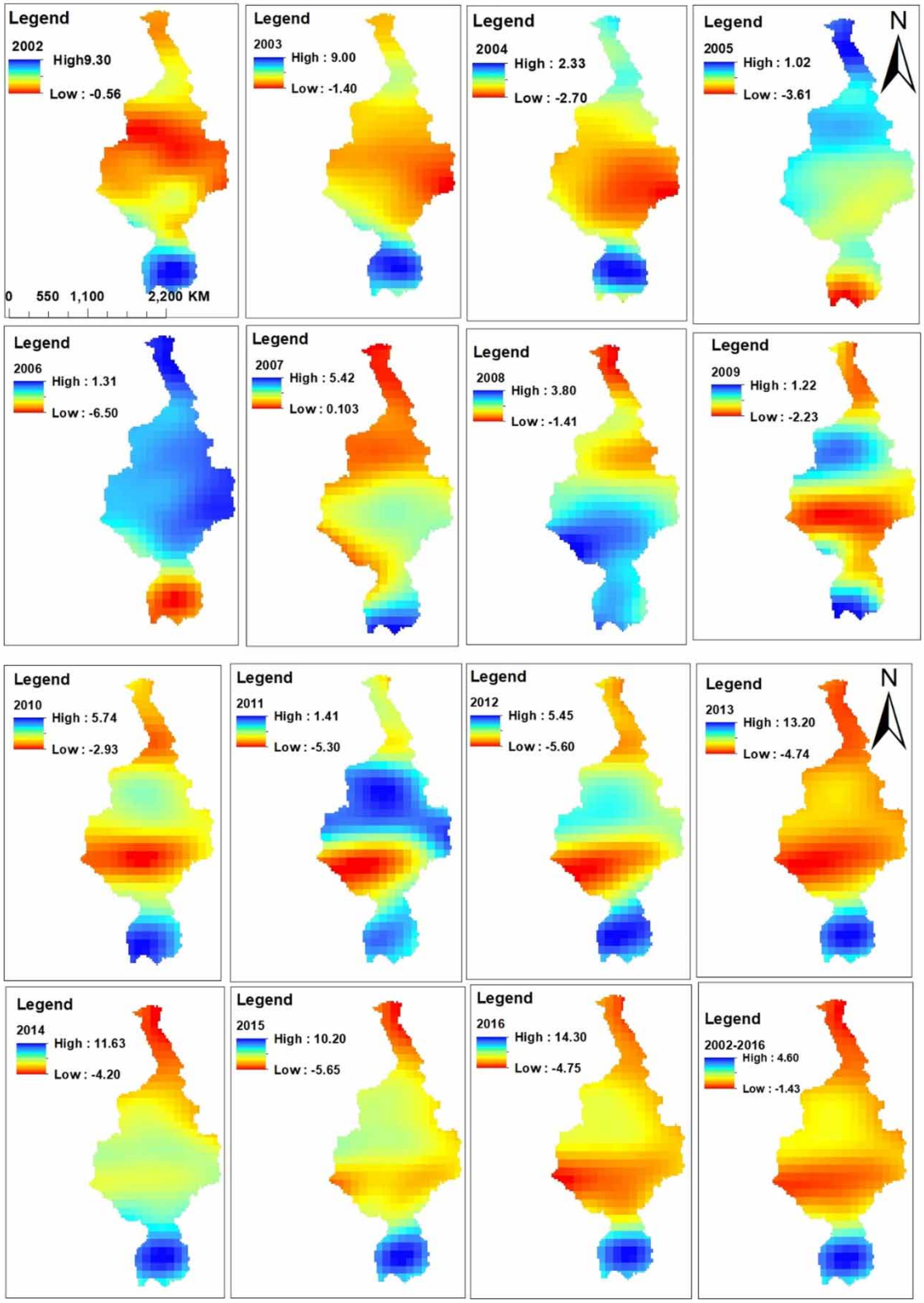

Figure 6 | The average annual variation of GRACE-based TWS for the Nile River basin from 2002 to 2016 in cm/year: The red color shows low water storage, and the blue color shows high water storage.

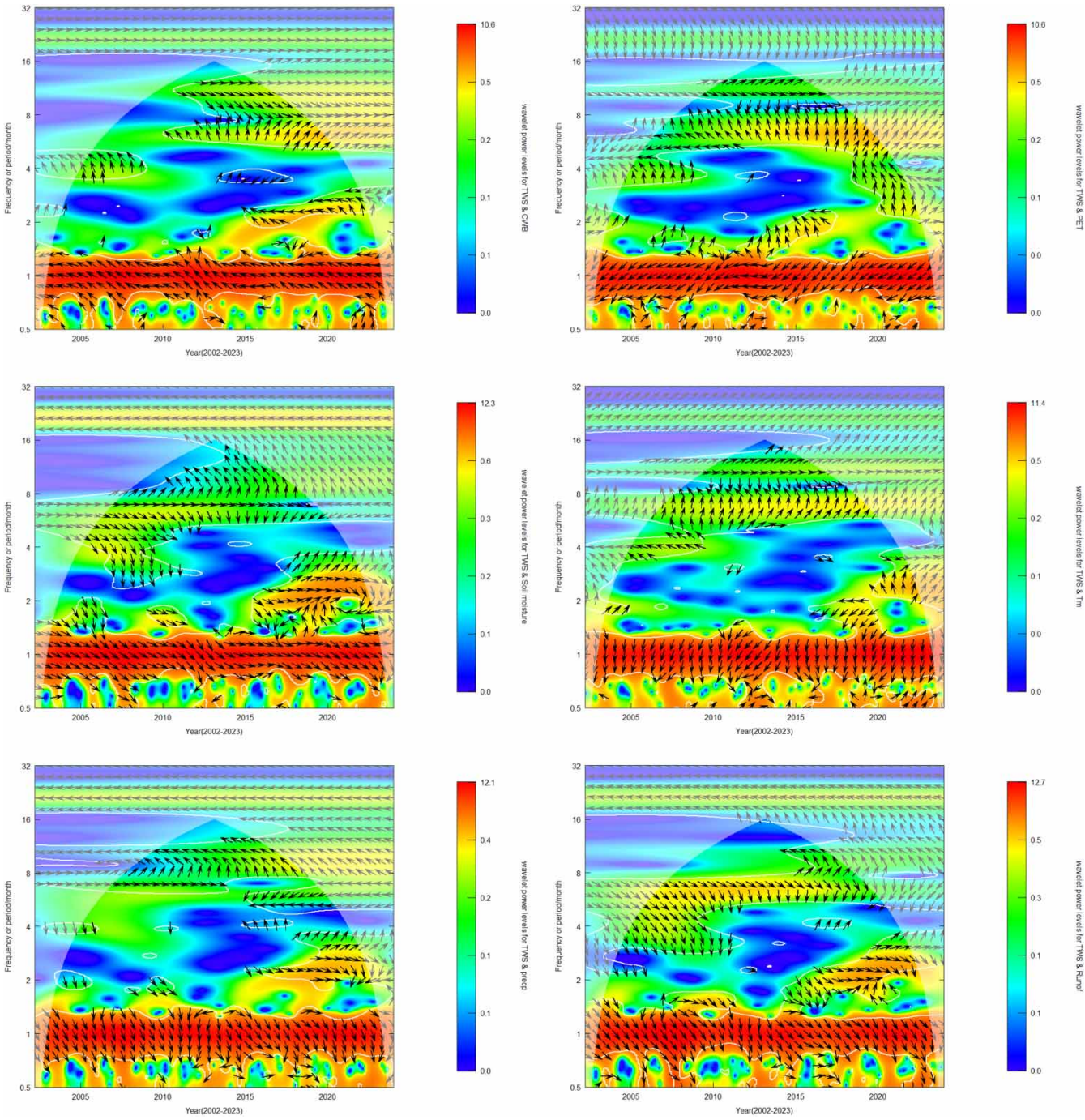

Figure 7 | Linkage between GRACE-TWS and climate parameters.

GRACE satellite data with higher-order statistical independent component analysis to explore these linkages (Anyah *et al.* 2018; Wei *et al.* 2021). The comparative time series analysis to correlate and link between the GRACE-based TWS and climate factors using correlation and the cross-wavelet transform method for this study provides new prospects and improved understanding of the TWSC in the Nile River and agrees with similar studies (Anyah *et al.* 2018; Wei *et al.* 2021). Furthermore, GRACE observations include both climatic variability and anthropogenic interventions, making it difficult to directly link GRACE signals to meteorological variability or human impacts.

3.5. Evaluation of drought indices in the Nile River basin

3.5.1. GRACE-derived drought index

Based on the evaluated WSD from GRACE-TWS, GDI was evaluated using Equation (2) and standardized using R-Studio, and the evaluated results are presented in Figure 8. Analysis shows that the Nile River basin experienced continuous drought between 2002 and 2019, and after July 2019, the water storage was predominantly in surplus. The WSD index detects severe hydrological drought in the Nile River basin. A severe peak drought was observed in 2009 with a magnitude of −2.62, with longer durations of drought observed between September 2003 and June 2007 and between August 2008 and September 2012. From the perspective of drought events of Thomas *et al.* (2014), 12 drought events were observed based on WSD between 2002 and 2023 in the Nile River basin (Supplementary material S2). Of the 12 confirmed drought events, the periods between October 2003 and July 2007 and between September 2008 and September 2012 were the most extensive drought periods in the study region, with durations of 45 and 49 months, respectively. The magnitude of the peak deficit was −2.6, observed in November 2009 (labeled as event No. 1), and the magnitude of the peak deficit was −1.93, observed in May 2013 (labeled as event No. 2). The highest total GDI was observed between September 2008 and September 2012 with a value of −16.2, whereas the minimum severe total drought was observed in 2013 with a value of 0.2. The results reveal that the WSD estimated by GRACE-TWS affords suitable insight for real-time hydrological drought estimation, which detected severe hydrological drought in the Nile River basin. The drought severity categories reflect the water storage deficiency in the study area, and the identified drought events have different magnitudes and durations. The estimated GRACE-TWS variation is due to seasonal water mass movement that can be influenced both by human intervention and natural variability due to the variability of precipitation and other factors. According to Getahun *et al.* (2021), the increase in temperature in the Indian Ocean resulted in decreased precipitation in East Africa. The change in precipitation leads to significant increases, decreases, and seasonality in TWS in the Nile River basin during this study, which is similar to other studies conducted in the Blue Nile basin (Ahmed *et al.* 2014; Hasan & Tarhule 2019; Hasan *et al.* 2019).

3.6. Meteorological drought indices

The study shows SPI, GDI, SPEI, and cumulative water deficit (CWD) in the Nile River basin during the study period (Figure 9). As shown in Figure 9, the results of the study showed that there was a continuous drought observed in the study area. For the SPI drought index, the severity of drought was observed in January 2012 with a peak value of −2.74. For RDI severity, drought was observed in August 2023 with a peak value of −1.77; for cumulative water deficit index (CWDI) severity, drought was observed in April 2014 with a peak value of −2.41; and for SPEI severity, drought was observed in October 2019 with a peak value of −3.15. According to the findings, SPI and RDI show similar trends after 2020 with little variation, whereas CWD and SPEI show similar trends during the study period. The results obtained for SPEI, SPI, CWDI, and RDI varied in length and severity of drought and peak period and are consistent with the findings reported by previous studies (Nigatu *et al.* 2021, 2024). It is clear that climate change and human activities are the main reasons that result in drought in the

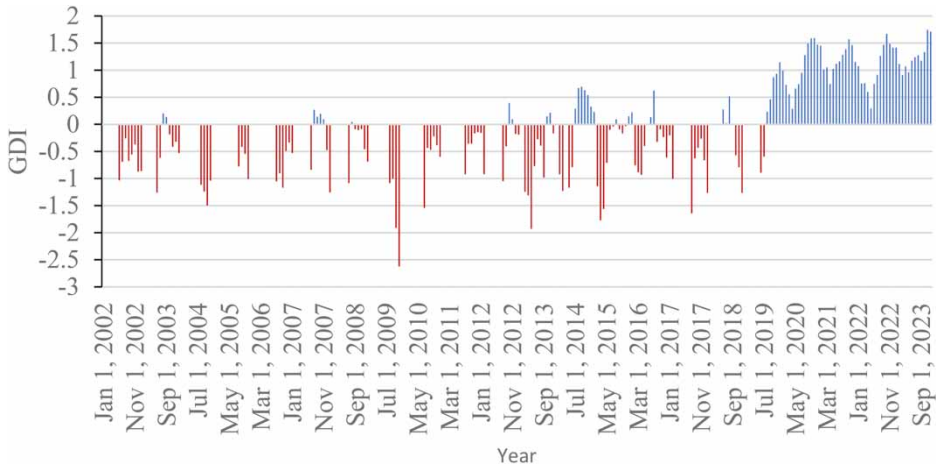

Figure 8 | GDI for the Nile River basin between 2002 and 2023.

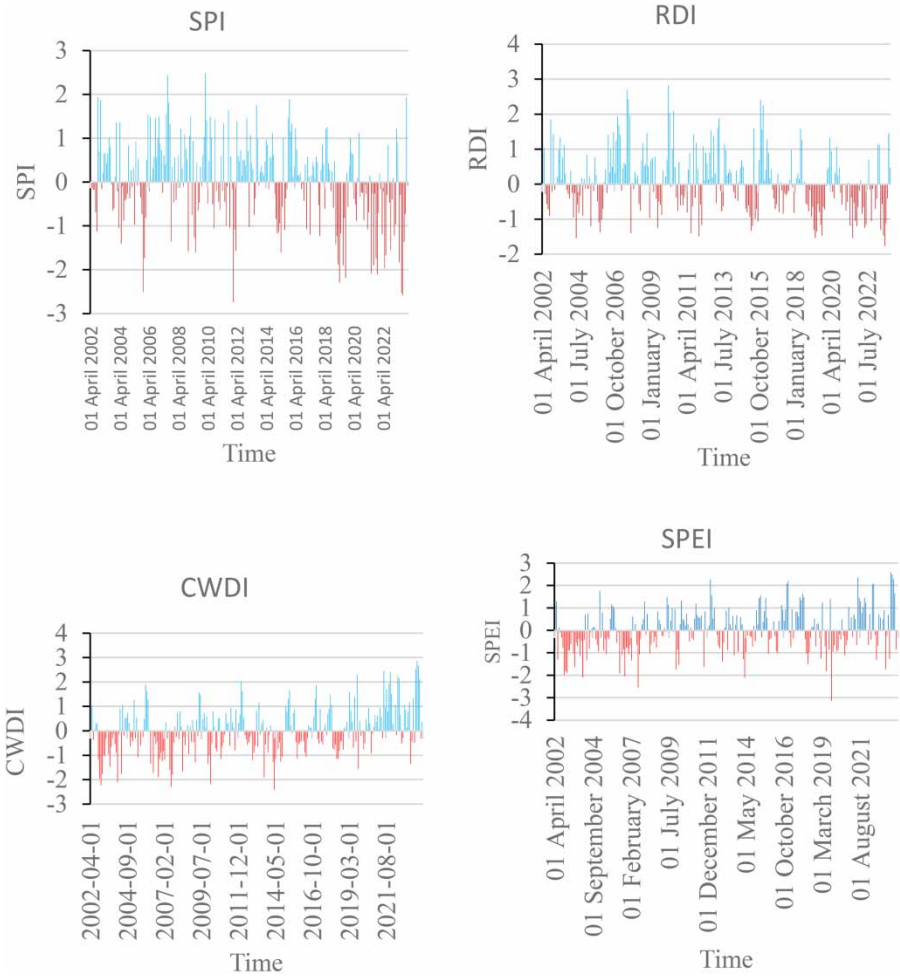

Figure 9 | Meteorological drought index.

study area. Climate change has impacted freshwater resources and put many places around the world at risk of development. Based on climate studies, Osima *et al.* (2018) reported an increase in temperatures leading to a rise in the Nile River basin. Therefore, considering the effect of temperature in the research area, the same research examined that the Nile River basin temperatures warm more quickly than the world mean temperature. The severity of the evaluated SPEI drought is associated with evaporative water demand because of evapotranspiration and has also been confirmed by different studies (Vicente-Serrano *et al.* 2010; Homdee *et al.* 2016). Human activities have changed land use and land cover in the Nile River basin, with an increase in urbanization and agricultural development due to the growing population in the river basin. These changes are expected to result in climate change and affect river basin management (Wu *et al.* 2022). Moreover, urbanization leads to an increase in impervious area, which in turn alters the distribution of precipitation, increases surface runoff, etc. With the progression of economic development, there has been a notable rise in water withdrawal for various water-use sectors such as irrigation, industry, and domestic use. This trend has direct consequences, including the decline in surface runoff, which increases the likelihood of extreme drought occurrences. Furthermore, the impact of human activities is more significant for water resource change due to the seasonal patterns of water withdrawals and the cyclical nature of reservoir operations. Ajwang (2023) evaluated the specific human activities on the Mau Complex and the Lake Victoria drainage system and their overall effect on the Nile basin and reported deforestation due to human activities.

3.7. Comparison of different drought patterns

The multiscale relationship between the GDI and the corresponding SPI, SPEI, CWDI, and SRI was detected using the cross-wavelet spectrum to understand its correlations and revealed how precipitation patterns, evapotranspiration, runoff,

temperature, and other climatic factors at different time scales affect water storage. Figure 10 shows the relationship between GDI, CWDI, SPI, SPEI, and RDI for the study area during the study period and observed in-phase, anti-phase, leading, and lagging correlations between GDI and the commonly used drought index throughout the study period. Based on the result, seven significant frequency periods were observed from 0.5 to 32 between GDI and the commonly used drought index. The correlation reflected a variation in the hydrological cycle process. According to the water balance, changes in TWS are a comprehensive reflection of changes in precipitation, evaporation, runoff, soil moisture, teleconnection factors, and anthropogenic factors such as land use, land cover change, irrigation practices, and others. The TWS is a crucial indicator of regional water resource changes triggered by the natural water cycle. Hydrologic drought caused by insufficient TWS is influenced by water storage components, contributing to the decreasing trend in TWS. These components will exacerbate the drought. Conversely, the water storage components that contribute to the increasing trend of TWS will mitigate or suppress the drought. The direction of the arrow, with anticorrelation pointing left and positive correlation going right, is used to represent the relative phase relationship between the drought indices. The left-to-right arrows show that the GDI coincided with the shift in the hydrological drought, whereas the right-to-left arrows show the negative correlation of the GDI with the selected drought index. The drought that occurs between 0.5 and 2 cycles is shown by the vertically upward or downward arrows, respectively, demonstrating a nonlinear association. The color of a cross-wavelet plot usually indicates the intensity or degree of the covariance between two signals at various frequencies and time scales, with a thick contour representing a

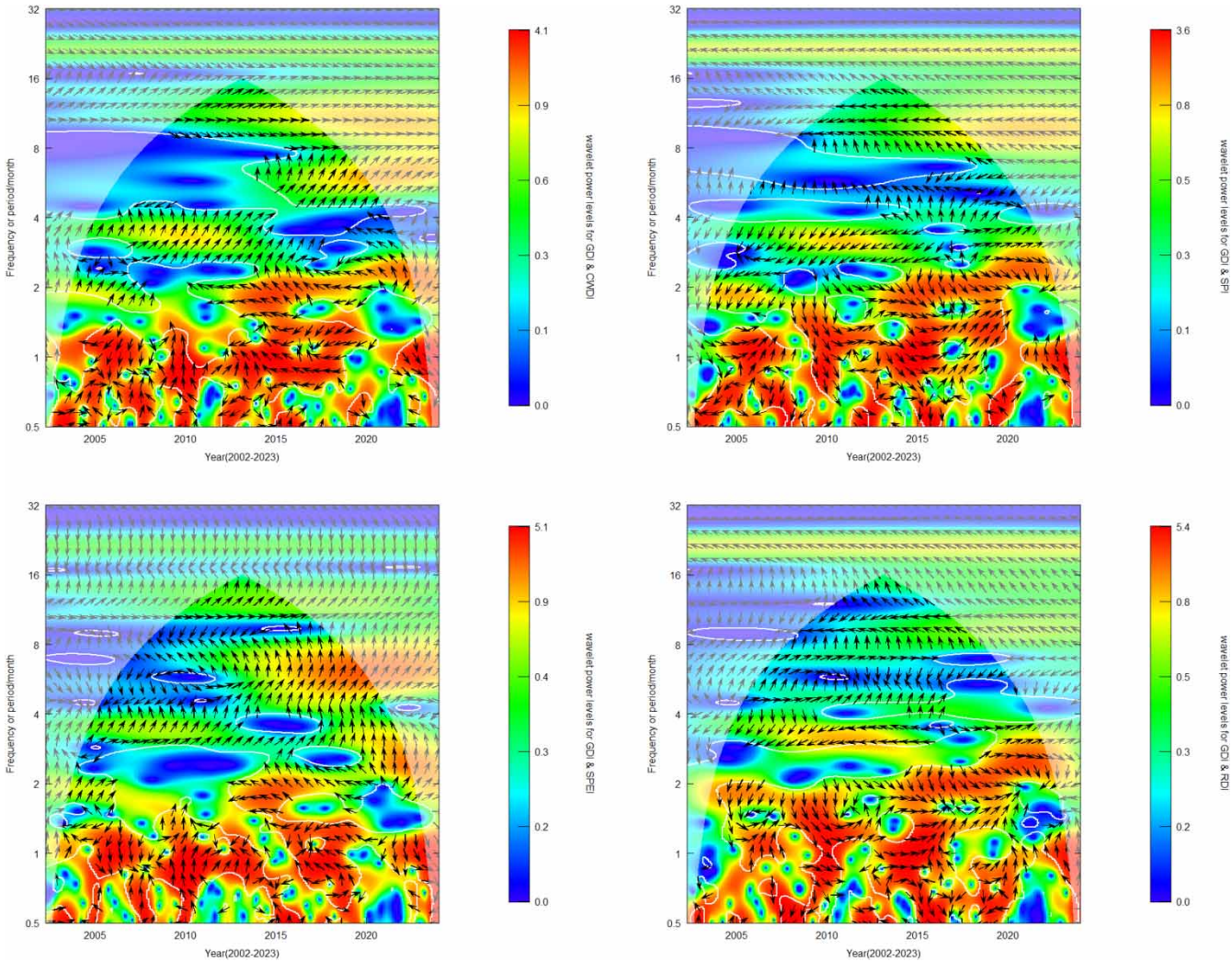

Figure 10 | The multiscale relationship between the GDI and the corresponding SPI, SPEI, CWDI, and SRI using the cross-wavelet method.

95% confidence level against red noise, with arrows indicating the relative phase connection of the drought index, whereas a low contour represents low color intensity. So, the dynamic linkages between the GDI and the corresponding drought index in the study area can be efficiently shown by the cross-wavelet transform and have a statistically significant association, suggesting that GRACE-based TWS was crucial to identifying the drought index. Therefore, the study shows a strong correlation between observed GRACE variability on year-to-year and multi-year timescales with climatic factors and also agrees with similar studies (Vergni *et al.* 2021).

3.8. The correlation of GRDI and meteorological drought indices

Climate change and the growing demand for freshwater have raised the frequency and intensity of extreme events like drought. Satellite observations have improved our understanding of the temporal and spatial variability of droughts. Since March 2002, the Gravity Recovery and Climate Experiment (GRACE) and its successor GRACE Follow-On (GRACE-FO) have been observing variations in the Earth's gravity field, yielding valuable information about changes in TWSA. TWS vertically integrates all forms of water on and beneath the land surface, including snow, surface water, soil moisture, and groundwater storage. Drought indices help to monitor drought by characterizing it in terms of its severity, location, duration, and timing. The correlation of GDI with other commonly used drought indices (SPEI, RDI, CWDI, and SPI) was evaluated. The estimated drought characteristics use the water deficit time series distribution compared with hydrometeorological drought indices. The result of GDI is consistent with all hydrometeorological droughts throughout the study area and proposes that GDI is suitable for identifying long-term hydrological drought, which can be successfully employed to evaluate hydrological drought. The evaluated cross-correlation between SPEI and SPI is 0.927; GDI and SPI were 0.868, GDI and SPEI were 0.867, GDI and RDI were 0.790, and GDI and GWDI were 0.868. This shows that hydrological drought has a high cross-correlation with GDI. Sensitivity analysis plays a crucial role in understanding the behavior and reliability of both GRACE-based drought indices and meteorological drought indices. GRACE (Gravity Recovery and Climate Experiment) is sensitive to changes in TWS, including groundwater, soil moisture, and surface water. This sensitivity allows it to detect hydrological and agricultural droughts. A GDI was developed based on the concept behind conventional drought indices. Sensory analysis reveals how climate-related or anthropogenic water storage trends can mask drought signals in GRACE analysis. Studies aim to understand how drought signals propagate through GRACE drought indicators in the presence of linear trends, constant accelerations, and GRACE-specific spatial noise. The robustness of GRACE-based drought indices is affected by several factors. Linear trends and constant accelerations in GRACE data tend to mask drought signals. Different spatial averaging methods, required to suppress spatially correlated GRACE noise, also affect the outcome. The sensitivity analysis of meteorological drought indices examines their response to drought conditions and various record-length and hydroclimatic factors. The robustness of meteorological drought indices is influenced by various factors, like soil moisture, vapor pressure deficit, solar radiation, atmospheric carbon dioxide concentration in vegetation in response to drought, and others. Studies aim to understand how drought signals propagate through GRACE drought indicators in the presence of linear trends, constant accelerations, and GRACE-specific spatial noise, and meteorological drought propagates due to soil moisture, vapor pressure deficit, solar radiation, and atmospheric activities (Gerdener *et al.* 2020; Vishwakarma 2020; Wang *et al.* 2020; Viet & Thuy 2024).

3.9. Discussion

This study describes the estimation of drought using GRACE-TWS. The three GRACE data products were used to evaluate TWS deficits in the Nile River basin to characterize drought manifestation. Drought assessments and monitoring using GRACE satellite datasets have been evaluated for the study area, especially where ground-based observed datasets are not sufficient. Recent advancements in satellite remote sensing have helped to generate new datasets that are used to propose new drought indices. For the evaluation of GDI, first, the water storage variation from GRACE was smoothed by Gaussian smoothing, and then, the water storage averaging of the three data products was carried out. The missing data were filled using linear interpolation methods during the study period. Based on the estimated result, continuous changes in water storage were observed in the study area internally. The study shows that the water storage in the study area shows an abrupt increase between 2017 and 2024. The maximum water storage value was observed in 2023, and the minimum value of water storage was observed in 2009 with values of 265.25 and −7.66 cm/year, respectively. In this study, the negative value of TWS indicates the WSD, whereas the positive value of TWS shows the water storage surplus. For the evaluation of GDI, the WSD was evaluated from the evaluated terrestrial storage by subtracting the average value of TWS from

GRACE time series data using Equation (1). The WSD result indicates that the study area has been experiencing a WSD and surpluses based on seasonal variation in the study area.

Generally, based on the evaluated results, variation in TWS and WSD was observed in the study area. This variation is due to changes in water balance components, such as precipitation change, evapotranspiration, surface runoff, soil moisture, and others that are changed as a result of global warming, which will lead to hydrological changes. The variability of TWS with a change in water storage components was evaluated using wavelet computation and temperature. It was obtained that the variability of precipitation, temperature, evapotranspiration, runoff, soil moisture, and other factors leads to changes in water storage in the study area, and a similar study also reported that climate parameters are the main parameters for the variation in TWS (Wu *et al.* 2022; Zeray Öztürk 2022; Yoshe 2023, 2024a, b). Additionally, human activities such as urbanization, industrial development, irrigation agriculture, and construction of reservoirs can affect water storage in the study area and are confirmed by similar studies (Xie *et al.* 2019; Ajwang 2023).

The wavelet power level between TWS and CWB and TWS and PET ranges between 0 and 10.6; precipitation and TWS (0–12.1), TWS and runoff (0–12.7), TWS and soil moisture (0–12.3), and between TWS and Tm (0–11.4). For the relationship between TWS and each climate variable, the maximum wavelet power level was observed between 0.5 and 2 frequency periods. This result shows that TWS was affected due to the periodic oscillation of climate variables, and different studies also show that climate change was the main reason for the variability of WSC.

The analysis of GDI shows that the Nile River basin experienced continuous drought between 2002 and 2019, which was due to the variation of water balance components and also as a result of global warming, which will lead to hydrological drought, and agreed with similar findings (Wu *et al.* 2022), but after July 2019, the water storage was predominantly in surplus in the study area.

From the perspective of drought evaluation, 12 drought events were observed because of WSD between 2002 and 2023 in the Nile River basin. Of the 12 confirmed drought events, the periods between October 2003 and July 2007 and between September 2008 and September 2012 were the most extensive drought periods in the study region, with durations of 45 and 49 months, respectively.

A severe peak drought was observed in 2009 with a magnitude of −2.62, with longer durations of drought observed between September 2003 and June 2007, and August 2008 and September 2012. The highest total GDI was observed between September 2008 and September 2012, with a value of −16.2, whereas the minimum severe total drought was observed in 2013, with a value of 0.2. Therefore, the WSD from GRACE detects severe hydrological drought throughout the study area, and the GRACE-TWS affords suitable insight for real-time hydrological drought evaluation. As a result, the evaluated GDI significantly correlated with meteorological drought.

The linkage between GDI and other commonly used drought indices throughout the study period shows that in-phase, anti-phase, leading, and lagging correlations. Based on the result, different significant frequency periods were observed from 0.5 to 32 between GDI and the commonly used drought index. Therefore, remote sensing approaches are cost-effective and efficient to quantify droughts at different scales and agree with similar studies (Yirdaw *et al.* 2008; Chen *et al.* 2009; Frappart *et al.* 2012; Long *et al.* 2013; Sun *et al.* 2018; Sinha *et al.* 2019; Yu *et al.* 2019). Therefore, a recently proposed drought assessment, as well as characterization using satellite information, is crucial to provide important information for resource management, along with supplementing the previous studies. As a result, the consecutive significant deficits in rainfall and change in temperature were the main cause of drought for the study area, which agrees with previous studies (Nigatu *et al.* 2024). The complex linkages between various drought occurrences, providing insight into their frequency and temporal aspects, were evaluated. The variation of water balance components, such as precipitation change, evapotranspiration, surface runoff, soil moisture, and others, is changed as a result of global warming, which will lead to hydrological drought. Flash droughts intensified during the global warming phase as a result of higher soil moisture drying trends and rapid ET, which resulted in more severe drought events and is consistent with other studies (Wang *et al.* 2016). The comparative time series analysis to correlate and link between the GRACE-based TWS and climate factors using correlation and the cross-wavelet transform method for this study provides new prospects and improved understanding of the TWSC in the Nile River and agrees with similar studies (Anyah *et al.* 2018; Scanlon *et al.* 2021; Wei *et al.* 2021). The multiscale relationship between the GDI and the corresponding SPI, SPEI, CWDI, and SRI was detected using the cross-wavelet spectrum to understand its correlations and revealed how precipitation patterns, evapotranspiration, runoff, temperature, and other climatic factors at different time scales affect water storage. The direction of the arrow, with anticorrelation pointing left and positive correlation going right, is used to represent the relative phase relationship between the drought indices. The left-to-right arrows show that the GDI

coincided with the shift in the hydrological drought, whereas the right-to-left arrows show the negative correlation of the GDI with the selected drought index.

The drought that occurs between 0.5 and 2 cycles is shown by the vertically upward or downward arrows, respectively, demonstrating a nonlinear association. The color of a cross-wavelet plot usually indicates the intensity or degree of the covariance between two signals at various frequencies and time scales, with a thick contour representing a 95% confidence level against red noise, with arrows indicating the relative phase connection of the drought index, whereas a low contour represents low color intensity. The robustness of GDIs is affected by several factors. Linear trends and constant accelerations in GRACE data tend to mask drought signals. The sensitivity analysis of meteorological drought indices examines their response to drought conditions and various record lengths and hydroclimatic factors. The robustness of meteorological drought indices is influenced by various factors, like soil moisture, vapor pressure deficit, solar radiation, atmospheric carbon dioxide concentration in vegetation in response to drought, and others.

4. LIMITATIONS

GRACE data, while valuable for drought analysis, has limitations due to its coarse spatial resolution, which restricts its use at local scales. Additionally, errors in satellite measurements and signal leakage can affect the accuracy of drought assessments. While GRACE provides insights into terrestrial WSC, it's crucial to acknowledge these limitations and consider them when interpreting results, especially for smaller regions or when comparing with *in-situ* data.

5. CONCLUSIONS

In this study, WSD was evaluated from GRACE-derived TWSA and utilized to evaluate drought index in the Nile River basin from 2002 to 2023. Based on the obtained result, a continual deficit of water storage during the study period was observed in the Nile River basin. Additionally, the cross-wavelet coherence analysis was applied to further identify the possible multiscale relationships between GRACE-TWS and the corresponding climate variables in the Nile River basin. Based on the estimated WSD, 12 drought events were observed between 2002 and 2023 in the Nile River basin, and out of the 12 confirmed drought events, the periods between October 2003 and July 2007 and between September 2008 and September 2012 were the most extensive drought periods in the study region, with durations of 45 and 49 months, respectively. Additionally, other drought indices like SPI, SPEI, RDI, and CWDI were evaluated during the study period from 2002 to 2023. For each drought index, the duration of drought, average drought, total drought, and peak drought were evaluated on a 1-month drought timescale. For the evaluated drought indices, more extreme and severe drought events were observed for each drought index at different periods, and all drought indices follow a similar trend. The multiscale relationship between the GDI and the corresponding SPI, SPEI, CWBDI, and SRI was detected using the cross-wavelet spectrum to understand its correlations. The evaluated GDI significantly correlated with meteorological drought. Finally, this study verified the importance of utilizing GRACE data for drought quantification and characterization. The evaluated result of drought indices, their severity, and the duration of the drought were essential for water resource management, which provided a reliable outcome for the establishment of climate change adaptation pathways, and were essential for the mitigation of drought hazards in the study area.

DATA AVAILABILITY STATEMENT

Data cannot be made publicly available; readers should contact the corresponding author for details.

CONFLICT OF INTEREST

The authors declare there is no conflict.

REFERENCES

Abatzoglou, J. T., Williams, A. P., Boschetti, L., Zubkova, M. & Kolden, C. A. (2018) Global patterns of interannual climate fire relationships, *Global Change Biology*, **24** (11), 5164–5175. https://doi.org/10.1111/gcb.14405.

Abd-Elbaky, M. & Jin, S. (2019) Hydrological mass variations in the Nile River basin from GRACE and hydrological models, *Geodesy and Geodynamics*, **10** (6), 430–438. https://doi.org/10.1016/j.geog.2019.07.004.

AghaKouchak, A. (2015) A multivariate approach for persistence-based drought prediction: application to the 2010–2011 East Africa drought, *Journal of Hydrology*, **526**, 127–135. https://doi.org/10.1016/j.jhydrol.2014.09.063.

Ahmed, M., Sultan, M., Wahr, J. & Yan, E. (2014) The use of GRACE data to monitor natural and anthropogenic induced variations in water availability across Africa, *Earth Science Reviews*, **136**, 289–300. https://doi.org/10.1016/j.earscirev.2014.05.0.

Ajwang, N. (2023) Effects of human activities on the Nile Basin: lessons from Kenya, *Open Journal of Social Sciences*, **11**, 23–31. doi: 10.4236/jss.2023.111003.

Alizadeh, M. R. & Nikoo, M. R. (2018) A fusion-based methodology for meteorological drought estimation using remote sensing data, *Remote Sensing of Environment*, **211**, 229–247. doi:10.1016/j.rse.2018.04.001.

Anyah, R. O., Forootan, E., Awange, J. L. & Khaki, M. (2018) Understanding linkages between global climate indices and terrestrial water storage changes over Africa using GRACE products, *Science of The Total Environment*, **635**, 1405–1416. https://doi.org/10.1016/j.scitotenv.2018.04.159.

Bayissa, Y., Moges, S., Melesse, A., Tadesse, T., Abiy, A. Z. & Worqlul, A. (2021) Multi-dimensional drought assessment in Abbay/Upper Blue Nile Basin: the importance of shared management and regional coordination efforts for mitigation, *Remote Sensing*, **13**, 1835. https://doi.org/10.3390/rs13091835.

Beguería, S., Vicente-Serrano, S. M., Reig, F. & Latorre, B. (2014) Standardized precipitation evapotranspiration index (SPEI) revisited: parameter fitting, evapotranspiration models, tools, datasets and drought monitoring, *International Journal of Climatology*, **34** (10), 3001–3023. https://doi.org/10.1002/joc.3887.

Cacciamani, C., Morgillo, A., Marchesi, S. & Pavan, V. (2007) Monitoring and forecasting drought on a regional scale: Emilia-Romagna region methods and tools for drought analysis and management. In: Singh V. P. (ed.) *Water Science and Technology Library*, vol. 62. Dordrecht: Springer, Chapter 2, pp. 29–48.

Camberlin, P., (2009) Nile basin climates. In: Dumont, H. J. (ed.) *The Nile: Origin, Environments, Limnology and Human Use*. Dordrecht: Springer, pp. 307–333.

Cammalleri, C., Barbosa, P. & Vogt, J. V. (2019) Analyzing the relationship between multiple-timescale SPI and GRACE terrestrial water storage in the framework of drought monitoring, *Water*, **11** (8), 1672. https://doi.org/10.3390/w11081672.

Chao, B. F. & Ding, H. (2016) Global geodynamic changes induced by all major earthquakes, 1976–2015, *Journal of Geophysical Research: Solid Earth*, **121**, 8987–8999. doi:10.1002/2016JB013161.

Chen, J. L., Wilson, C. R., Tapley, B. D., Yang, Z. L. & Niu, G. Y. (2009) 2005 drought event in the Amazon River basin as measured by GRACE and estimated by climate models, *Journal of Geophysical Research*, **114** (B5), B05404. https://doi.org/10.1029/2008JB006056.

Creutzfeldt, B., Ferré, T., Troch, P., Merz, B., Wziontek, H. & Güntner, A. (2012) Total water storage dynamics in response to climate variability and extremes: inference from long-term terrestrial gravity measurement, *Journal of Geophysical Research: Atmospheres*, **117**, D08112. doi:10.1029/2011JD016472.

Dabanli, I. (2018) Drought hazard, vulnerability, and risk assessment in Turkey, *Arabian Journal of Geosciences*, **11**, 538. doi:10.1007/s12517-018-3867-x.

Dostdar, H., Aftab, A., Syed, N., Syed, A. & Akhtar, J. (2021) A time series assessment of terrestrial water storage and its relationship with hydro-meteorological factors in Gilgit-Baltistan region using GRACE observation and GLDAS-Noah model, *SN Applied Sciences*, **3**, 533. https://doi.org/10.1007/s42452-021-04525-4.

Elsaka, B. (2021) Evaluation of terrestrial total water height variations over the Nile River basin based on two full-years of GRACE-FO gravity field monthly solutions, *International Research Journal of Advanced Engineering and Science*, **6**, 90–95.

Elsaka, B., Abdelmohsen, K., Alshehri, F., Zaki, A. & ElAshquer, M. (2022) Mass variations in terrestrial water storage over the Nile River basin and mega aquifer system as deduced from GRACE-FO level-2 products and precipitation patterns from GPCP data, *Water*, **14** (23), 3920. https://doi.org/10.3390/w14233920.

Espinosa, L. A., Portela, M. M. & Rodrigues, R. (2019) Spatio-temporal variability of droughts over past 80 years in Madeira Island, *Journal of Hydrology: Regional Studies*, **25**, 100623. https://doi.org/10.1016/j.ejrh.2019.100623.

Farge, M. (1992) Wavelet transforms and their applications to turbulence, *Annual Review of Fluid Mechanics*, **24** (1), 395–458. https://doi.org/10.1146/annurev.fl.24.010192.002143.

Forootan, E., Khandu, J., Awange, J., Schumacher, M., Anyah, R., van Dijk, A. I. J. M. & Kusche, J. (2016) Quantifying the impacts of ENSO and IOD on rain gauge and remotely sensed precipitation products over Australia, *Remote Sensing of Environment*, **172**, 50–66. https://doi.org/10.1016/j.rse.2015.10.027.

Frappart, F., Papa, F., Santos Da Silva, J., Ramillien, G., Prigent, C., Seyler, F. & Calmant, S. (2012) Surface freshwater storage and dynamics in the Amazon basin during the 2005 exceptional drought, *Environmental Research Letters*, **7** (4), 044010. https://doi.org/10.1088/1748-9326/7/4/044010.

Gao, H., Korn, J. M., Ferretti, S., Monahan, J. E., Wang, Y., Singh, M., Zhang, C., Schnell, C., Yang, G., Zhang, Y., Balbin, O. A., Barbe, S., Cai, H., Casey, F., Chatterjee, S., Chiang, D. Y., Chuai, S., Cogan, S. M., Collins, S. D., Dammassa, E., Ebel, N., Embry, M., Green, J., Kauffmann, A., Kowal, C., Leary, R. J., Lehar, J., Liang, Y., Loo, A., Lorenzana, E., Robert McDonald 3rd., E., , McLaughlin, M. E., Merkin, J., Meyer, R., Naylor, T. L., Patawaran, M., Reddy, A., Röelli, C., Ruddy, D. A., Salangsang, F., Santacroce, F., Singh, A. P., Tang, Y., Tinetto, W., Tobler, S., Velazquez, R., Venkatesan, K., Von Arx, F., Wang, H. Q., Wang, Z., Wiesmann, M., Wyss, D., Xu, F., Bitter, H., Atadja, P., Lees, E., Hofmann, F., Li, E., Keen, N., Cozens, R., Jensen, M. R., Pryer, N. K., Williams, J. A. & Sellers, W. R. (2015) High-throughput screening using patient-derived tumor xenografts to predict clinical trial drug response, *Nature Medicine*, **21** (11), 1318–1325. doi: 10.1038/nm.3954. Epub 2015 Oct 19. PMID: 26479923.

Gerdener, H., Engels, O. & Kusche, J. (2020) A framework for deriving drought indicators from the Gravity Recovery and Climate Experiment (GRACE), *Hydrology and Earth System Sciences*, **24**, 227–248. https://doi.org/10.5194/hess-24-227-2020.

Getahun, Y. S., Li, M.-H. & Pun, I.-F. (2021) Trend and change-point detection analyses of rainfall and temperature over the Awash River basin of Ethiopia, *Heliyon*, **7** (9), e08024. https://doi.org/10.1016/j.heliyon.2021.e08024.

Grinsted, A., Moore, J. C. & Jevrejeva, S. (2004) Application of the cross wavelet transform and wavelet coherence to geophysical time series, *Nonlinear Processes in Geophysics*, **11** (5/6), 561–566. https://doi.org/10.5194/npg-11-561-2004.

Gudmundsson, L. & Stagge, J. H. (2016) Standardized Climate Indices Such as SPI, SRI or SPEI. V.1.0-2. 2016. Available at: https://cran.r-project.org/web/packages/SCI/index.html (Accessed: 10 February 2025).

Hamouda, M., Nour El-Din, M. M. & Moursy, F. I. (2009) Vulnerability assessment of water resources systems in the Eastern Nile Basin, *Water Resources Management*, **23**, 2697–2725. doi:10.1007/s11269-009-9404-7.

Hasan, E. & Tarhule, A. (2019) Trend Dynamics of GRACE Terrestrial Water Storage in the Nile River Basin. Preprints, pp. 14–23. https://doi.org/10.20944/preprints201909.0042.v1.

Hasan, E., Tarhule, A., Hong, Y. & Moore, B. (2019) Assessment of physical water scarcity in Africa using GRACE and TRMM satellite data, *Remote Sensing*, **11** (8), 904. https://doi.org/10.3390/rs11080904.

Hayes, M. J., Wilhite, D. A. & Vanyarkho, O. V. (1999) Drought using the Standardized Precipitation Index, *Bulletin of the American Meteorological Society*, **80**, 429–438.

Hobbins, M. T., Wood, A., McEvoy, D. J., Huntington, J. L., Morton, C., Anderson, M. & Hain, C. (2016) The evaporative demand drought index. Part I: linking drought evolution to variations in evaporative demand, *Journal of Hydrometeorology*, **17** (6), 1745–1761. https://doi. org/10.1175/JHM-D-15-0121.1.

Homdee, T., Pongput, K. & Kanae, S. (2016) A comparative performance analysis of three standardized climatic drought indices in the Chi River basin, Thailand, *Agriculture and Natural Resources*, **50** (3), 211–219. https://doi.org/10.1016/j.anres.2016.02.002.

Ji, L. A. & Peters, J. (2003) Assessing vegetation response to drought in the northern Great Plains using vegetation and drought indices, *Remote Sensing of Environment*, **87** (1), 85–98. https://doi.org/10.1016/S0034-4257(03)00174-3.

Keyantash, J. A. & Dracup, J. A. (2004) An aggregate drought index: assessing drought severity based on fluctuations in the hydrologic cycle and surface water storage, *Water Resources Research*, **40**, W09304. doi:10.1029/2003WR002610.

Landerer, F. W. & Swenson, S. C. (2012) Accuracy of scaled GRACE terrestrial water storage estimates, *Water Resources Research*, **48**, W04531. 11. doi:10.1029/2011WR011453.

Leblanc, M. J., Tregoning, P., Ramillien, G., Tweed, S. O. & Fakes, A. (2009) Basin-scale, integrated observations of the early 21st century multiyear drought in southeast Australia, *Water Resources Research*, **45**, W04408. doi:10.1029/2008WR007333.

Li, X., Pan, X. Y., Yang, M. Y., Yang, S. L., Fan, H. Y. & Zhang, Z. Q. (2021) Spatial and temporal characteristics of drought in Beijing based on multiple scale SPEI index, *Water Resources and Hydropower Engineering*, **11**, 50–63.

Liu, W. B., Fu, G. B. & Ouyang, R. L. (2012) A discussion of some aspects of statistical downscaling in climate impacts assessment, *Advances in Water Science*, **23**, 427–437 (in Chinese).

Long, D., Scanlon, B. R., Longuevergne, L., Sun, A. Y., Fernando, D. N. & Save, H. (2013) GRACE satellite monitoring of large depletion in water storage in response to the 2011 drought in Texas, *Geophysical Research Letters*, **40** (13), 3395–3401. https://doi.org/10.1002/grl.50655.

Long, D., Pan, Y., Zhou, J., Chen, Y., Hou, X., Hong, Y., Scanlon, B. R. & Longuevergne, L. (2017) Global analysis of spatiotemporal variability in merged total water storage changes using multiple GRACE products and global hydrological models, *Remote Sensing of Environment*, **192**, 198–216. doi:10.1016/j.rse.2017.02.011.

McKee, T. B., Doesken, N. J. & Kleist, J. (1993) *The Relationship of Drought Frequency and Duration to Time Scales*, 8th Conference on Applied Climatology, Anaheim, 17–22 January 1993, pp. 179–184. Available at: http://citeseerx.ist.psu.edu/viewdoc/summary?doi ¼ 10.1.1.462.4342.

Mera, G. A. (2018) Drought and its impacts in Ethiopia. *Weather and Climate Extremes*. Elsevier B.V. https://doi.org/10.1016/j.wace.2018.10.002.

Munagapati, H., Yadav, R. & Tiwari, V. M. (2018) Identifying water storage variation in Krishna Basin, India from in situ and satellite based hydrological data, *Journal of the Geological Society India*, **92** (5), 607–615. https://doi.org/10.1007/s12594-018-1074-8.

Niemeyer, S. (2008) New drought indices, *Options Méditerranéennes. Série A: SéminairesMéditerranéens*, **80**, 267–274.

Nigatu, Z. M., Fan, D., You, W. & Melesse, A. M. (2021) Hydroclimatic extremes evaluation using GRACE/GRACE-FO and multidecadal climatic variables over the Nile River basin, *Remote Sensing*, **13**, 651. doi:10.3390/rs13040651.

Nigatu, Z. M., You, W. & Melesse, A. M. (2024) Drought dynamics in the Nile River basin: meteorological, agricultural, and groundwater drought propagation, *Remote Sensing*, **16** (5), 919. https://doi.org/10.3390/rs16050919.

Onyutha, C. & Willems, P. (2015a) Spatial and temporal variability of rainfall in the Nile Basin, *Hydrology and Earth System Sciences*, **19**, 2227–2246. doi:10.5194/hess-19-2227-2015.

Osima, S., Indasi, V. S., Zaroug, M., Endris, H. S., Gudoshava, M., Misiani, H. O., Nimusiima, A., Anyah, R. O., Otieno, G., Ogwang, B. A., Jain, S., Kondowe, A. L., Mwangi, E., Lennard, C., Nikulin, G. & Dosio, A. (2018) Projected climate over the Greater Horn of Africa under 1.5 °C and 2 °C global warming, *Environmental Research Letters*, **13**, 065004. doi:10.1088/1748-9326/aaba1b.

Palazzoli, I., Ceola, S. & Gentine, P. (2025) GR*Ai*CE: reconstructing terrestrial water storage anomalies with recurrent neural networks, *Scientific Data*, **12**, 146. https://doi.org/10.1038/s41597-025-04403-3.

Pendergrass, A. G., Meehl, G. A., Pulwarty, R., Hobbins, M., Hoell, A., AghaKouchak, A., Bonfils, C. J. W., Gallant, A. J. E., Hoerling, M., Hoffmann, D., Kaatz, L., Lehner, F., Llewellyn, D., Mote, P., Neale, R. B., Overpeck, J. T., Sheffield, A., Stahl, K., Svoboda, M., Wheeler, M. C., Wood, A. W. & Woodhouse, C. A. (2020) Flash droughts present a new challenge for subseasonal-to-seasonal prediction, *Nature Climate Change*, **10**, 191–199. https://doi.org/10.1038/s41558-020-0709-0.

Philipps, J. & McIntyre, B. (2000) ENSO and interannual rainfall variability in Uganda: implications for agricultural management, *International Journal of Climatology*, **20**, 171–182.

Richey, A. S., Thomas, B. F., Lo, M. H., Reager, J. T., Famiglietti, J. S., Voss, K., Swenson, S. & Rodell, M. (2015) Quantifying renewable groundwater stress with GRACE, *Water Resources Research*, **52**, 4184–4187.

Rummel, R. J. (1976) *Understanding Correlation*. Honolulu, HI: University of Hawaii. p. 1. Available at: http://www.mega.nu:8080/ampp/rummel/uc.htm.

Scanlon, B. R., Rateb, A., Pool, D. R., Sanford, W., Save, H., Sun, A., Long, D. & Fuchs, B. (2021) Effects of climate and irrigation on GRACE-based estimates of water storage changes in major US aquifers, *Environmental Research Letters*, **16**, 9. doi: 10.1088/1748-9326/ac16ff.

Segele, Z. T. & Lamb, P. J. (2005) Characterization and variability of Kiremt rainy season over Ethiopia, *Meteorology and Atmospheric Physics*, **89**, 153–180. doi:10.1007/s00703-005-0127-x.

Seka, A. M., Zhang, J., Zhang, D., Ayele, E. G., Han, J., Prodhan, F. A., Zhang, G. & Liu, Q. (2022) Hydrological drought evaluation using GRACE satellite-based drought index over the lake basins, East Africa, *Science of The Total Environment*, **852**, 158425. doi: 10.1016/j.scitotenv.2022.158425. Epub 2022 Sep 5. PMID: 36063925.

Seyoum, W. M., Kwon, D. & Milewski, A. M. (2019) Downscaling GRACE TWSA data into high-resolution groundwater level anomaly using machine learning-based models in a glacial aquifer system, *Remote Sensing*, **11**, 824. doi:10.3390/rs11070824.

Shukla, S. & Wood, A. (2008) Use of a standardized runoff index for characterizing hydrologic drought, *Geophysical Research Letters*, **35**, 1–7. L02405. doi:10.1029/2007GL032487.

Sinha, D., Syed, T. H., Famiglietti, J. S., Reager, J. T. & Thomas, R. C. (2019) Characterizing drought in India using GRACE observations of terrestrial water storage deficit, *Journal of Hydrometeorology*, **18** (2), 381–396. https://doi.org/10.1175/JHM-D-16-0047.1.

Stanke, C., Kerac, M., Prudhomme, C., Medlock, J. & Murray, V. (2013) Health effects of drought: a systematic review of the evidence, *PLoS Currents*, **5**.

Sun, Z., Zhu, X., Pan, Y., Zhang, J. & Liu, X. (2018) Drought evaluation using the GRACE terrestrial water storage deficit over the Yangtze River Basin, China, *Science of the Total Environment*, **634**, 727–738. https://doi.org/10.1016/j.scitotenv.2018.03.292.

Swenson, S. C. (2012) GRACE monthly land water mass grids NETCDF RELEASE 5.0. Ver. 5.0. PO.DAAC, CA, USA. https://doi.org/10.5067/TELND-NC005.

Swenson, S. C. & Wahr, J. M. (2002) Methods for inferring regional surface-mass anomalies from Gravity Recovery and Climate Experiment (GRACE) measurements of time-variable gravity, *Journal of Geophysical Research: Solid Earth*, **107**, 2193.

Swenson, S. C. & Wahr, J. (2006) Post-processing removal of correlated errors in GRACE data, *Geophysical Research Letters*, **33**, L08402. doi:10.1029/2005GL025285.

Tapley, B. D., Bettadpur, S., Ries, J. C., Thompson, P. F. & Watkins, M. M. (2004) GRACE measurements of mass variability in the earth system, *Science*, **305**, 503–505. doi:10.1126/science.1099192.

Tapley, B. D., Watkins, M. M., Flechtner, F., Reigber, C., Bettadpur, S., Rodell, M., Sasgen, I., Famiglietti, J. S., Landerer, F. W., Chambers, D. P., Reager, J. T., Gardner, A. S., Save, H., Ivins, E. R., Swenson, S. C., Boening, C., Dahle, C., Wiese, D. N., Dobslaw, H., Tamisiea, M. E. & Velicogna, I. (2019) Contributions of GRACE to understanding climate change, *Nature Climate Change*, **9**, 358–369. doi:10.1038/s41558-019-0456-2.

Thomas, J. & Prasannakumar, V. (2016) Temporal analysis of rainfall (1871–2012) and drought characteristics over a tropical monsoon dominated State (Kerala) of India, *Journal of Hydrology*, **534**, 266–280. https://doi.org/10.1016/j.jhydrol.2016.01.013.

Thomas, A. C., Reager, J. T., Famiglietti, J. S. & Rodell, M. (2014) A GRACE-based water storage deficit approach for hydrological drought characterization, *Geophysical Research Letters*, **41**, 1537–1545. doi:10.1002/2014GL059323.

Tsakiris, G., Pangalou, D. & Vangelis, H. (2007) Regional drought assessment based on the Reconnaissance Drought Index (RDI), *Water Resources Management*, **21** (5), 821–833. doi:10.1007/s11269-006-9105-4.

Valiya Veettil, A. & Mishra, A. K. (2020) Multiscale hydrological drought analysis: role of climate, catchment and morphological variables and associated thresholds, *Journal of Hydrology*, **582**, 124533. doi:10.1016/j.jhydrol.2019.124533.

Vergni, L., Todisco, F. & Di Lena, B. (2021) Evaluation of the similarity between drought indices by correlation analysis and Cohen's Kappa test in a Mediterranean area, *Natural Hazards*, **108**, 2187–2209. doi:10.1007/s11069-021-04775-w.

Vicente-Serrano, S. M., Beguería, S. & López-Moreno, J. I. (2010) A multiscalar drought index sensitive to global warming: the standardized precipitation evapotranspiration index, *Journal of Climate*, **23**, 1696–1718. doi:10.1175/2009JCLI2909.1.

Viet, L. V. & Thuy, T. T. T. (2024) Drought sensitivity analysis of meteorological and vegetation indices in Dak Nong, Vietnam, *Journal of Water and Climate Change*, **15** (10), 4968–4988. https://doi.org/10.2166/wcc.2024.661.

Vishwakarma, B. D. (2020) Monitoring droughts from GRACE, *Frontiers in Environmental Science*, **8**, 584690. https://doi.org/10.3389/fenvs.2020.584690.

Wahr, J., Swenson, S., Zlotnicki, V. & Velicogna, I. (2004) Time-variable gravity from GRACE: first results, *Geophysical Research Letters*, **31**, L11501. doi:10.1029/2004GL019779.

Wang, J., Jiang, D., Huang, Y. & Wang, H. (2014) Drought analysis of the Haihe River basin based on GRACE terrestrial water storage, *Scientific World Journal*, **2014**, 578372.

Wang, W., Cui, W., Wang, X. & Chen, X. (2016) Evaluation of GLDAS-1 and GLDAS-2 forcing data and Noah model simulations over China at the monthly scale, *Journal of Hydrometeorology*, **17**, 2815–2833. doi:10.1175/JHM-D-15-0191.1.

Wang, L., Kaban, M. K., Thomas, M., Chen, C. & Ma, X. (2019) The challenge of spatial resolutions for GRACE-based estimates volume changes of larger man-made lake: the case of China's Three Gorges Reservoir in the Yangtze River, *Remote Sensing*, **11** (1), 99. https://doi.org/10.3390/rs11010099.

Wang, F., Wang, Z., Yang, H., Di, D., Zhao, Y. & Liang, Q. (2020) Utilizing GRACE-based groundwater drought index for drought characterization and teleconnection factors analysis in the North China Plain, *Journal of Hydrology*, **585**, 124849. https://doi.org/10.1016/j.jhydrol.2020.124849.

Wei, L., Jiang, S., Ren, L., Tan, H., Ta, W., Liu, Y., Yang, X., Zhang, L. & Duan, Z. (2021) Spatiotemporal changes of terrestrial water storage and possible causes in the closed Qaidam Basin, China using GRACE and GRACE Follow-On data, *Journal of Hydrology*, **598**, 126274. https://doi.org/10.1016/j.jhydrol.2021.126274.

WMO (2012) World Meteorological Organization. In: Svoboda, M., Hayes, M. & Wood, D. (eds.) *Standardized Precipitation Index User Guide*. Geneva, Switzerland: WMO-No. 1090; WMO, p. 16. Available at: https://library.wmo.int/doc_num.php?explnum_id=7768.

Wu, T., Zheng, W., Yin, W. & Zhang, H. (2021) Spatiotemporal characteristics of drought and driving factors based on the GRACE derived total storage deficit index: a case study in southwest China, *Remote Sensing*, **13**, 79. doi:10.3390/rs13010079.

Wu, G., Chen, J., Shi, X., Kim, J. S., Xia, J. & Zhang, L. (2022) Impacts of global climate warming on meteorological and hydrological droughts and their propagations, *Earth's Future*, **10**, e2021EF002542. doi:10.1029/2021EF002542.

Xie, J., Xu, Y., Wang, Y., Gu, H., Wang, F. & Pan, S. (2019) Influences of climatic variability and human activities on terrestrial water storage variations across the Yellow River basin in the recent decade, *Journal of Hydrology*, **579**, 124218. doi:10.1016/j.jhydrol.2019.124218.

Yi, H. & Wen, L. (2016) Satellite gravity measurement monitoring terrestrial water storage change and drought in the continental United States, *Scientific Reports*, **6**, 19909. doi:10.1038/srep19909.

Yihdego, Y., Vaheddoost, B. & Al-Weshah, R. A. (2019) Drought indices and indicators revisited, *Arabian Journal of Geosciences*, **12**, 69. doi:10.1007/s12517-019-4237-z.

Yirdaw, S. Z., Snelgrove, K. R. & Agboma, C. O. (2008) GRACE satellite observations of terrestrial moisture changes for drought characterization in the Canadian Prairie, *Journal of Hydrology*, **356** (1–2), 84–92. https://doi.org/10.1016/j.jhydrol.2008.04.004.

Yoshe, A. K. (2023) Estimation of change in terrestrial water storage for Abbay River Basin, Ethiopia, *Hydrology Research*, **54** (11), 1451–1475. https://doi.org/10.2166/nh.2023.119.

Yoshe, A. K. (2024a) Assessment of anthropogenic and climate-driven water storage variations over water-stressed river basins of Ethiopia, *Hydrology Research*, **55** (3), 351–379. https://doi.org/10.2166/nh.2024.169.

Yoshe, A. K. (2024b) Water availability identification from GRACE dataset and GLDAS hydrological model over data-scarce river basins of Ethiopia, *Hydrological Sciences Journal*, **69** (6), 721–745. https://doi.org/10.1080/02626667.2024.2333852.

Yoshe, A. K. (2025) Integrated study of GRACE-based groundwater storage variability across Ethiopia for sustainable economic development, *African Geographical Review*, 1–24. https://doi.org/10.1080/19376812.2025.2528730.

Yu, W., Li, Y., Cao, Y. & Schillerberg, T. (2019) Drought assessment using GRACE terrestrial water storage deficit in Mongolia from 2002 to 2017, *Water*, **11** (6), 1301. https://doi.org/10.3390/w11061301.

Zargar, A., Sadiq, R., Naser, B. & Khan, F. I. (2011) A review of drought indices, *Environmental Reviews*, **19**, 333–349. doi:10.1139/a11-013.

Zeray Öztürk, E. (2022) Evaluation of water storage changes in Southeastern Anatolia, Turkey, using GRACE and GLDAS, *Meteorology Hydrology and Water Management*, **10** (1), 47–59. https://doi.org/10.26491/mhwm/149849.

Zhang, D., Zhang, Q., Werner, A. D. & Liu, X. (2016) GRACE-based hydrological drought evaluation of the Yangtze River basin, China, *Journal of Hydrometeorology*, **17** (3), 811–828. doi:10.1175/JHM-D-15-0084.1.

Zhang, X., Li, J., Wang, Z. & Dong, Q. (2022) Global hydroclimatic drivers of terrestrial water storage changes in different climates, *CATENA*, **219**, 106598. https://doi.org/10.1016/j.catena.2022.106598.

Zhao, M., Velicogna, I. & Kimball, J. S. (2017) Satellite observations of regional drought severity in the continental United States using GRACE-based terrestrial water storage changes, *Journal of Climate*, **30**, 6297–6308. doi:10.1175/JCLI-D-16-0458.1.

Zhong, Y., Feng, W., Humphrey, V. & Zhong, M. (2019) Human-induced and climate-driven contributions to water storage variations in the Haihe River Basin, China, *Remote Sensing*, **11**, 3050.

First received 23 December 2024; accepted in revised form 9 October 2025. Available online 29 October 2025